Canada Basin hydrography in the CESM-LE and observations: implications for vertical ocean heat transport in a transitioning sea ice cover

Juliette Lavoie[1], Bruno Tremblay[1], Erica Rosenblum[2]

[1]Atmospheric and Oceanic Sciences Department, McGill University, Montreal, QC, Canada
[2]Centre for Earth Observation Science, University of Manitoba, Winnipeg, Manitoba, Canada

Key Points:

- The CESM-LE is missing heat from Pacific Waters which should create 1.4m of reduced winter ice growth over 3 years
- During the transition to a seasonal ice cover, the stratification weakens in the CESM-LE, contrary to the increase in the observations

Corresponding author: Juliette Lavoie, juliette.lavoie@mail.mcgill.ca

Abstract

In recent years, there has been a significant sea ice retreat in the Pacific sector of the Arctic. One possible cause is the increase in ocean heat flux amplified by the ice-albedo feedback. This paper looks at vertical ocean heat transport from waters of Pacific origin and solar heat into the mixed layer and their impact on the sea ice mass balance in the Community Earth System Model - Large Ensemble (CESM-LE). To this end, we focus on two specific periods with observational hydrographic data from the Arctic Ice Dynamics Joint Experiment (1975-76) and Ice-Tethered Profiler (2004-2018). A comparison between simulated and observed salinity and potential temperature profiles highlights two key model biases in all ensemble members: an absence of Pacific Waters in the water column and a deepening of the winter mixed layer in opposition to observations that show a reduction in depth of the mixed layer and a stronger increase in stratification. Results from a one-dimensional vertical heat budget show that remnant solar heat trapped beneath the halocline is mostly ventilated to the surface by mixing before the following melt season, while vertical advection associated with Ekman pumping, even in early fall when the winds are strong and the pack-ice is weak, only has a small effect on the vertical heat transport. Furthermore, we estimate from the 1D heat budget a reduction of 1.4 m winter ice growth over three years (the residence time of ice in the Beaufort Gyre) associated with the missing Pacific Waters.

Plain Language Summary

In recent years, the Arctic has lost a lot of ice, especially in the Pacific Sector. One possible explanation for this loss is a change in the heat coming from the ocean below the ice. In this paper, we use observations of temperature and salinity and a global climate model to study where the heat is under the ice and how it moves during two periods: before (1970s) and during (2000s) the large loss of ice. There are two big differences between the observations and the model. First, in the observations, the large ice melt deposits freshwater on top of the ocean which creates large stratification that reduces the vertical mixing, while in the model, with the same ice loss, the vertical mixing is increased. Second, the model is missing some heat from the Pacific Ocean which could reduce the growth of ice in the winter by 1.4 m in three years.

1 Introduction

The Arctic has witnessed record retreat of sea ice extent (SIE) in recent years with the largest loss of ice in the Pacific sector (Beaufort and Chukchi Seas) (Fetterer, F. et al., 2017; McLaughlin et al., 2011). This is unexpected because thick multiyear ice north of the Canadian Arctic Archipelago is being recicurlated in the Pacific Sector through the Beaufort Gyre – although, a more cyclonic ice circulation in the Canada Basin associated with a low bias in sea level pressure could explain some of the decline in the Pacific Sector (DeRepentigny et al., 2016). Early signs of this Pacific-centric retreat were present even in 1997-98, when a thick multi-year ice floe, needed to set up the *Surface Heat Budget of the Arctic Ocean* (SHEBA) camp, proved difficult to find (Curry, 1999). There is not yet a consensus for the cause of loss of multi-year ice in the Beaufort and Chukchi Seas. Possible causes include an increase in vertical heat flux in the Canada Basin (CB) (Carmack et al., 2015; Woodgate et al., 2010; Steele et al., 2010; Peterson et al., 2017; Maslowski et al., 2012), a trend in sea ice thickness from Arctic warming amplified by the ice-albedo feedback (Perovich, Jones, et al., 2011), a trend in coastal divergence in the Beaufort Sea (Kim et al., 2021), and increased ocean heat flux in the Bering Strait (Lenetsky et al., 2021). While the observed Pacific-centric retreat of the pack ice is in agreement with 10 members of the Community Earth System Model-Large Ensemble (CESM-LE) and this model's predecessor the Community Climate System Model (CCSM) 4 (DeRepentigny et al., 2016; Desmarais & Tremblay, 2021), whether the model has the

proper behavior for the correct reason remains unknown (Rosenblum & Eisenman, 2017). The goal of this paper is to investigate the influence of vertical ocean heat flux on the sea ice mass balance in the CESM-LE during the transition from a perennial sea ice cover to a seasonal ice cover, and comparing the model to the hydrographic data from Arctic Ice Dynamics Joint EXperiment (AIDJEX) in 1975-76 and Ice-Tethered Profilers (ITP) data in 2004-2018 – two periods before and after the beginning of the transition to a seasonally ice free Arctic.

In an early study, the mean annual flux from the ocean to the ice was estimated at $\sim$ 2 W m^{-2} from a 1D thermodynamic model constrained by observed surface radiative and turbulent fluxes from AIDJEX (Maykut & Untersteiner, 1971). Later, Maykut and McPhee (1995) showed that the ice-ocean heat flux has a strong seasonality with a negligible winter mean and a summer mean of 40-60 W m^{-2}. The ice-ocean turbulent flux is dependant on the temperature of the mixed layer. Factors that can modify this temperature include strong winds events, resulting in fluxes as high as $\sim$ 350 Wm^{-2} (Peterson et al., 2017), and changes in the bathymetry (Huwald et al., 2005). A major driver of the mixed layer temperature is the input of shortwave flux to the ocean surface. Indeed, shortwave flux penetrating the ocean is correlated to bottom melt via the ice-ocean flux (Perovich, Richter-Menge, et al., 2011). In recent years, the ice-ocean turbulent heat flux have increased substantially with more open water leading to a 4% per year increase in shortwave flux entering the ocean (Perovich et al., 2007). Vertical ocean heat flux from depth into the mixed layer also influences the ice-ocean heat flux and the sea ice mass balance.

In the Canada Basin, there are three main sources of heat beneath the surface mixed layer: the Near Surface Temperature Maximum (NSTM), the summer/winter Pacific Waters (PW) and the Atlantic Waters (AW). The NSTM is remnant solar heat trapped beneath the mixed layer at the onset of ice formation (Maykut & McPhee, 1995; Perovich et al., 2008; Jackson et al., 2010; Steele et al., 2011). Heat from the NSTM is ventilated during the fall and winter (Jackson et al., 2012) via convection associated with ice formation and brine rejection (Rudels et al., 1996; Timmermans, 2015) and enhanced turbulent mixing associated with inertial oscillations (Rainville et al., 2011). Warm PW enters through the Bering Strait and are divided into three branches: (i) The Alaskan Coastal Current (ACC), which penetrates the Canada Basin, the Canadian Arctic Archipelago (Yamamoto-Kawai et al., 2008), Lancaster and Jones sounds (Jones et al., 2003) or continues along the coast on the Shelfbreak Jet (Pickart, 2004) where eddies break off the shelf and enters the Canada Basin (Manley & Hunkins, 1985; Pickart et al., 2005); (ii) A second branch, which flows through the middle channel between Herald and Hanna Shoals and joins the ACC or flows over the shelf to the Canada Basin (Weingartner et al., 2005); (iii) A third branch, which reaches Herald Canyon and flows over the shelf in the Canada Basin (Ladd et al., 2016; Gong & Pickart, 2015). Warm and salty waters from the northern North Atlantic (AW) enter though the Fram Strait and the Barent Sea Opening, rejoin at the St Anna Trough and flow cyclonically around the Eurasian Basin into the Canada Basin (Nikolopoulos et al., 2009). However, this layer does not meaningfully impact the sea ice mass balance as vertical heat fluxes through double staircase diffusion in the Atlantic Waters layer remain small (0.1 W m^{-2}) (Timmermans et al., 2008).

Heat moves vertically through the water column via diffusion or advection. Advection by Ekman transport in the Canada Basin has an impact on the vertical stratification and, therefore, on vertical heat fluxes. Indeed, Steele et al. (2011) argue that the downwelling of the Beaufort Gyre is partly responsible for the survival of the NSTM in that region as it is pushed below the mixed layer depth. The anticyclonic winds cause a convergence of surface ocean waters. In turn, this leads to downwelling in the center of the Canada Basin of the order $\sim$1 myr^{-1}, particularly in the fall when the winds are strong and the pack ice still weak (Proshutinsky et al., 2009; Meneghello, Marshall, Timmermans, & Scott, 2018). Ekman convergence is balanced by eddy diffusion (Davis et al., 2014). Yet, Meneghello, Marshall, Campin, et al. (2018); Meneghello et al. (2020)

argue that the late winter thicker and slower ice cover drags the ocean acting as a governor, which removes the need for eddy diffusion to balance the gyre.

Diffusion moves heat from the NSTM and PW to the surface via small turbulence (Rudels et al., 1996), though the exact amount of diffusion is still debated (Shaw & Stanton, 2014; Jackson et al., 2012; Timmermans et al., 2008; Davis et al., 2016). Errors in vertical mixing can lead to errors in heat leaving the ocean by up to 50 Wm^{-2} (Goosse et al., 1999) and also in simulation of the Atlantic and Pacific Waters flowing cyclonically or anticyclonically in the Canada Basin (Zhang & Steele, 2007). In models, a proper representation of the halocline requires an accurate brine rejection parameterization as well as an accurate diffusivity with KPP parameterization (Nguyen et al., 2009; Large et al., 1994). Though, most climate models still have difficulties simulating accurate stratification (Holloway et al., 2007; Ilıcak et al., 2016; Rosenblum, Fajber, et al., 2021).

In the Arctic, the winter halocline is a permanent feature, sustained by lateral advection from the Eurasian shelf, as salt rejection from ice formation in the fall salinifies fresh shelf waters that find their level of equilibrium beneath the surface mixed layer (Aagaard et al., 1981). The halocline separates the fresher and colder surface waters from the generally warmer and saltier deeper layers. The stratification also has a seasonal cycle (Lemke & Manley, 1984; Morison & Smith, 1981): As ice melts in the summer, fresh water is released in the mixed layer creating a salinity profile with the seasonal halocline on top of the winter halocline (Rudels et al., 1996; Jackson et al., 2010). In the fall, the seasonal halocline erodes, while brine rejection from ice formation increases the salinity of the mixed layer (Lemke & Manley, 1984). Water temperature in the winter halocline can be near-freezing in the Eurasian Basin, referred to as the cold halocline layer, or cool in the Canada Basin where NSTM and PW are present beneath the mixed layer (Steele & Boyd, 1998). The strong gradient in salinity, together with the cold/cool halocline layer, creates a barrier that insulates the top of the ocean as salt rejection induced convection brings cold water to the surface, resulting in near zero vertical ocean heat flux. This contrasts the Southern Ocean where ice forms until the seasonal halocline is eroded (Aagaard et al., 1981; Rudels et al., 1996; Morison & Smith, 1981; Martinson, 1990).

Finally, the recent loss of ice in the Arctic is driving two competing mechanisms affecting the vertical heat transport: (1) reduced vertical mixing due to surface freshening and increased stratification, and (2) increased vertical mixing due to a thinner and more mobile pack ice. Hydrographic observations in the Canada Basin in recent decades clearly show a reduction of the mixed layer pointing to the dominance of increased stratification (Peralta-Ferriz & Woodgate, 2015). Whether these processes are well-represented in global climate models is crucial to understanding the evolution of the ice-ocean heat flux and sea ice mass balance.

Auclair and Tremblay (2018) found a link between ocean heat transport through the Bering Strait and rapid sea ice decline on the continental shelf in the CESM-LE. When the pack ice migrates northward over the deep ocean, rapid declines are caused instead by anomalies in radiative fluxes and ice transport. The goal of this paper is to assess the accuracy of the simulated vertical ocean heat flux in the retreat seen during the transition from a seasonal to a perennial ice cover over the deep basin. To this end, the simulation of the CESM-LE is analyzed compared to observations to assess the biases of the model (Holloway et al., 2007; Ilıcak et al., 2016; Rosenblum, Fajber, et al., 2021).

The paper is structured as follows. Section 2 presents the observations (2.1.1), the model (2.1.2) and the methods (2.2). Section 3 presents the results and discussion and is divided in three parts: (3.1) the bulk heat budget of the ice-ocean system, (3.2) the simulated and observed vertical profiles in the surface ocean, and (3.3) a 1D vertical heat transport budget. Section 4 presents a conclusion and summary of the results.

2 Data and Methods

2.1 Data

2.1.1 Observations: AIDJEX and ITP

We use Canada Basin temperature and salinity profiles from the AIDJEX (Moritz, Richard, 2020) and ITP (Krishfield et al., 2008), which were collected during 1975 - 1976 and 2004 - 2018, respectively (Figure 1). Profiles with data between 10 m - 490 m – range common to most profiles – were interpolated on a 1m resolution grid. AIDJEX consisted of four ice camps deployed between 75 − 78°N and 143 − 148° W in April 1975 that drifted southwest in the Beaufort Sea. ITP buoys selected for analysis cover the full Canada Basin (72−80°N and 130-155 °W). 36 ITPs were deployed in the period 2004-2018, taking measurements once or twice a day, each with an average life span of 260 days consisting of 15303 profiles. There is a large difference in the number of data points between AIDJEX and ITP. However, the differences between the periods highlighted in this paper by looking at averages remain true for a majority of profiles.

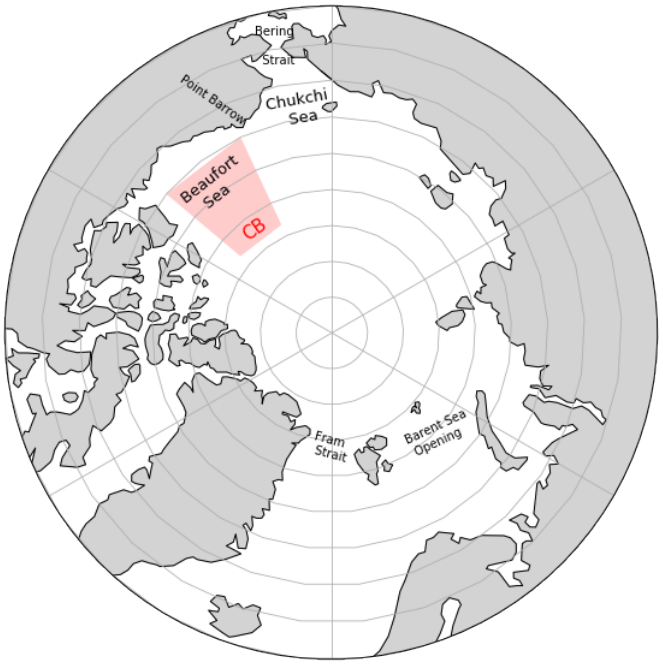

Figure 1. Arctic domain and definition of the Canada Basin (72−80°N and 130-155 °W). The blue dots are located at the center of each grid cell within the Basin in the native CESM grid.

2.1.2 Model: CESM-LE

The Community Earth System Model (CESM1) has four components. The sea ice component is the Community Ice CodE (CICE 4), which has four ice layers and one snow layer. It includes a subgrid-scale ice thickness distribution (ITD) (Bitz et al., 2001; Lipscomb, 2001), an energy conserving thermodynamics scheme that accounts for brine pockets (Bitz & Lipscomb, 1999) and an elastic-viscous-plastic rheology (Hunke & Dukowicz, 1997). The ITD has five ice categories: 0 m - 0.64 m - 1.39 m - 2.47 m - 4.57 m - ∞. The ocean component is the Parallel Ocean Project (POP 2), which has 60 vertical layers with a vertical resolution ranging from 10 m to 250 m at depth. It uses the K-profile parameterization (KPP) vertical mixing parameterization (Large et al., 1994),

the Gent-McWilliams parameterization for horizontal tracer diffusion (Gent & Mcwilliams, 1990), anisotropic horizontal viscosity (Large et al., 2001), and third-order upwind advection for tracers (Leonard, 1979). The freezing temperature is fixed at $-1.8°$C. The land component is the Community Land Model (CLM 4), which uses the SIMTOP scheme for drainage and sub-surface runoff (Niu et al., 2005). The atmosphere component is the Community Atmosphere Model (CAM 5), which has 30 layers and uses the Rapid Radiative Transfer Method (Iacono et al., 2008; Mlawer et al., 1997). All components have a nominal spatial resolution of 1°, resulting in an effective resolution of 40-70km in the Arctic. The pole of the ocean and ice grid is located over Greenland, in order to avoid the singularity at the pole. The Arakawa B-grid is used with tracers defined at the grid center and vectors defined on the vertices.

The CESM - Large Ensemble (CESM-LE) is a set of 40 ensemble members (EMs) - based on the CESM1 – differing only by a slightly varying initial conditions (Kay et al., 2015). The model was initialized using observed ocean temperature and salinity, as well as, atmosphere, land and sea ice conditions from an existing CESM1 run. It ran under constant pre-industrial forcing for 1500 years until the model reached equilibrium. The first ensemble member (EM1) was initialized from a random date of the constant 1850 forcing period and run for an additional 250 years. Other EMs were initialized with 1920 EM1 values and with a one day lag in ocean conditions (EM2) or a given random perturbations of the order of 10^{-14}K in the air temperatures (EM3-40). All EMs are run with observed CO_2 concentration from initialization to 2005 and with RCP8.5 from 2006 to 2100.

2.2 Methods

In section 3.2, the CESM-LE and ITP profiles are averaged over grid cell with SIC $> 60\%$ as the observations are biased toward cooler temperatures. When the ITP is in a zone of low ice concentration, it is biased towards cold temperature as it is attached below to a thicker floe. Hence, we compare model and observations for higher SIC (see Figure 2).

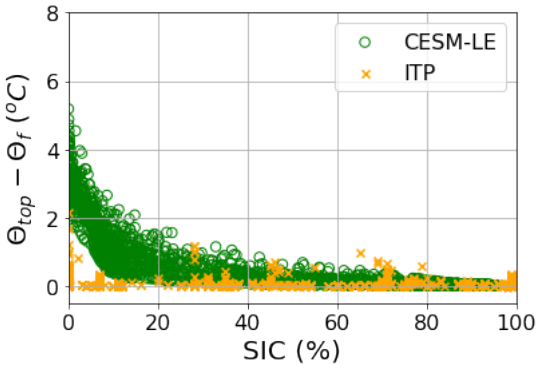

Figure 2. September top (valid value closest to the surface) temperature away from freezing vs. sea ice concentration (SIC) over the Canada Basin for ITP (yellow crosses) and the CESM-LE (green circles) (showing only one ensemble member as an example for clarity).

Next, the conservation energy equation is used to calculate a 1D (vertical) ocean heat budget over the top 200m.

$$\rho \frac{\partial e}{\partial t} + \rho w \frac{\partial e}{\partial z} = D + R, \tag{1}$$

where e ($= c_p\Theta$) is the internal energy per mass unit (J kg^{-1}), c_p is specific heat of sea water (J kg^{-1} °C^{-1}), Θ is the potential temperature (°C^{-1}), ρ is the density (kg m^{-3}), w is the vertical velocity (m s^{-1}), D is the vertical diffusion of heat (J s^{-1} m^{-3}), and R is the divergence of surface radiative fluxes (J s^{-1} m^{-3}).

The energy equation can be written in flux form using the continuity equation:

$$\frac{\partial \rho}{\partial t} + w\frac{\partial \rho}{\partial z} + \rho\frac{\partial w}{\partial z} = 0. \tag{2}$$

Multiplying eq. 2 by e and adding it to eq. 1 gives:

$$\frac{\partial E}{\partial t} = R + D - \frac{\partial (wE)}{\partial z}, \tag{3}$$

where $E = e\rho$ is the internal energy per volume unit (J m^{-3}). These four terms will be calculated from CESM-LE output as defined below. The 40 ensemble members are used to estimate the uncertainty in each term associated with natural variability.

The tendency for the internal energy is calculated using a second order centered finite difference scheme as

$$\left.\frac{\partial E}{\partial t}\right|_t = \frac{E_{t+1} - E_{t-1}}{2\Delta t}, \tag{4}$$

where $E(t)$ is monthly mean temperature for month t and Δt is the difference between two time steps (1 month). We use the monthly mean temperature because snapshots in the CESM-LE simulation are only stored every 5 years. This will lead to an error of $O(\Delta t^2)$ that will be discussed below in section 3.1.

The simulated divergence of surface fluxes (R) is given by

$$R = \begin{cases} \frac{\partial}{\partial z}\left(F_{sw,ao} + F_{sw,io} + F_{lw} + F_{sens} + F_{evap} + F_{frazil}\right), & \text{if } z = z_1 \\ \frac{\partial}{\partial z}\left(F_{sw,ao} + F_{sw,io}\right), & \text{otherwise,} \end{cases} \tag{5}$$

where z_1 is first layer at the top of the water column, $F_{sw} = F_{sw,ao} + F_{sw,io}$ is the shortwave flux (W m^{-2}), which penetrates the ocean directly from the atmosphere to the ocean (ao) and from the atmosphere through ice to the ocean (io), F_{lw} is the longwave flux (atmosphere/ocean), F_{sens} is the sensible heat flux (atmosphere/ocean), F_{evap} the latent heat flux from evaporation or deposition (atmosphere/ocean), and F_{frazil} is the latent heat from the formation of new ice in the ocean over open water, i.e. the heat required to warm the supercooled water ($\Theta < -1.8$°C) to freezing point temperature and is calculated as an equivalent downward heat flux by the CESM-LE. The simulated shortwave flux decays exponentially with depth following Beer's Law and chlorophyll levels, based on Ohlmann (2003). The longwave, sensible, evaporation, and frazil fluxes do not penetrate below the first layer, implying that $\frac{\partial F}{\partial z} = \frac{\Delta F}{\Delta z} = \frac{F}{\Delta z}$, where Δz is the thickness of the layer. Heat fluxes that lead to an increase in the ocean temperature are taken to be positive.

The simulated vertical diffusion of heat (D) is given by

$$D = \begin{cases} D_{VM} + D_{iso} + \frac{F_{io}}{\Delta z}, & \text{if } z = z_1. \\ D_{VM} + D_{iso}, & \text{otherwise,} \end{cases} \tag{6}$$

where D_{VM} is the vertical mixing from the KPP parameterization, D_{iso} is the vertical component of isopycnal mixing from the Gent-McWilliams parameterization, and F_{io} is the ice-ocean turbulent heat flux (which depends on the gradient of temperature between the ice base and the mixed layer, similar to D_{VM}),

$$F_{io} = \rho c_p c_h u_* (\Theta - \Theta_f), \tag{7}$$

where c_h is a heat transfer coefficient and u_* is the friction velocity.

D_{VM} is composed of a diabatic (D_{dia}) and a non-local term, (D_{nl})

$$D_{VM} = D_{dia} + D_{nl} = c_p \rho \left[\frac{\partial}{\partial z}(\kappa \frac{\partial \Theta}{\partial z}) - \frac{\partial}{\partial z}(\kappa \gamma_\Theta) \right], \tag{8}$$

where κ is the diffusivity and γ_Θ is the non-local vertical heat flux, which represents mixing associated with convection and unstable vertical stratification.

The error in the 1D heat budget is calculated from the residual, which includes non-resolved horizontal advection and diffusion as well as the error ($O(\Delta t^2)$) from the second order finite difference approximation of the time derivative.

Following Peralta-Ferriz and Woodgate (2015), the mixed layer depth (MLD) is calculated as the shallowest depth where the change in potential density ($\Delta\sigma$) is larger or equal to the 0.1 kg m^{-3} threshold.

$$\Delta\sigma = \sigma(z) - \sigma(z_{min}) \geq 0.1 kg m^{-3}, \tag{9}$$

where $z_m in$ is the shallowest measured depth.

The correspondence between the names of variables in this paper and their name in the CESM-LE is shown in the appendix (Table 1).

3 Results and Discussion

3.1 Heat Budget

To first order, the mean July 1970-1979 ice-ocean heat budget is a balance between the net solar radiation ($F_{sw,ao} = 29.77 \pm 2.98$ W m^{-2}), turbulent ice-ocean heat flux ($F_{io} = -22.74 \pm 1.94$ W m^{-2}), and the change in internal energy of the entire water column ($\frac{\partial E}{\partial t} = 9.22 \pm 1.76$ W m^{-2} – see figure 3. The sea ice mass balance is mainly controlled by thermodynamic effects, with a small contribution from ice export of $-3.73\pm$ 7.25 cm averaged over the summer. Integrated over the summer, the basal sea ice melt (60.11±7.14 cm), which is associated with the turbulent ice-ocean heat flux and a negligible contribution from the conductive heat flux, is larger than the surface melt (33.78± 5.82 cm; not shown). This is in general agreement with observations from AIDJEX (34 cm vs 26 cm for basal and surface melt respectively, Maykut & McPhee, 1995). However, the model differs from some earlier measurements made in the 1950s that have very large variabilty. For example, Untersteiner (1961) reports basal and surface melt of 22 cm vs 19 cm and 24 cm vs 41 cm in 1957 and 1958 from measurements made in the same region as part of the US Drifting Station A of the International Geophysical Year.

The second order terms in the July heat budget include solar flux transmitted through the ice ($F_{sw,io} = 5.69\pm0.94$ W m^{-2}), longwave cooling over open ocean ($F_{lw} = -4.14\pm$ 0.56 W m^{-2}), and lateral ocean heat transport ($F_{hor} = 1.90\pm0.79$ W m^{-2}). The main contribution of the lateral ocean heat transport is advection by the mean flow and eddies; the advection by sub-mesoscale eddies is negligible (results not shown). When considering all terms, the heat budget closes to within -1.33 ± 0.52 W m^{-2}, which is approximately 5% of the first order terms (F_{io} and $F_{sw,ao}$). This error mainly comes from the second order finite difference approximation of the internal energy tendency term ($\frac{\partial E}{\partial t}$) using the monthly mean ocean temperatures as opposed to instanteneous temperatures.

We find numerous differences between the July ice-ocean surface heat budget in 1970-1979 and 2010-2019. First, both the solar heat flux into the ocean and the ice-ocean turbulent heat flux is 40% larger in 2010-2019 than in 1970-1979. Second, the transmitted shortwave radiation through the snow/ice and the internal energy of the ocean both doubled. The larger transmitted shortwave radiation through the ice in 2010-2019 is due to reduced snow depth and ice thickness. The large increase in internal energy is due to a bias low in ice-ocean turbulent heat flux despite a large warming of the surface ocean and the absence of an increased in stratification with increased sea ice melt (see discus-

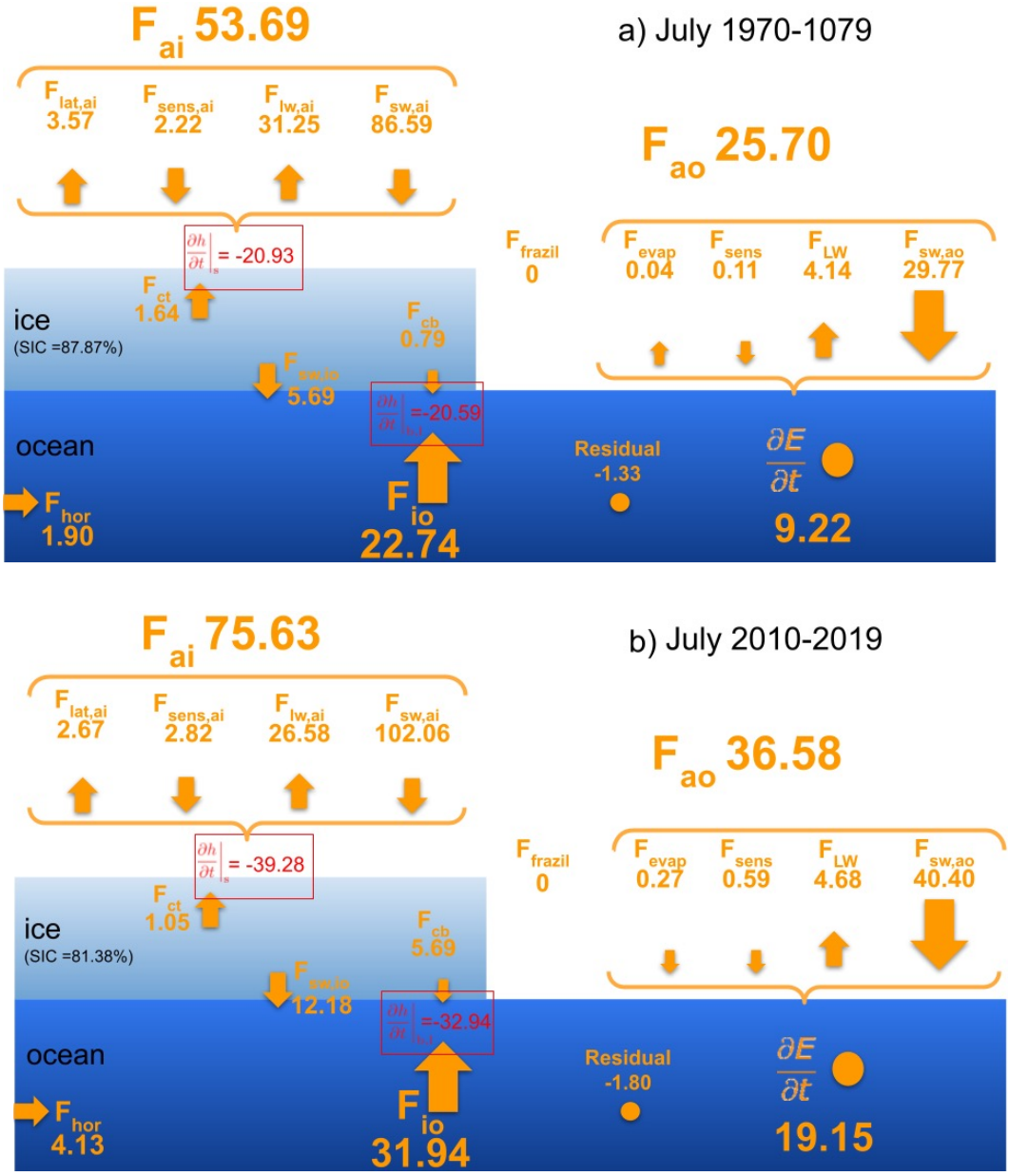

Figure 3. CESM-LE ensemble-mean ice-ocean heat budget for July averaged spatially over the Canada Basin and temporally over the years a) 1970-1979 or b) 2010-2019. Changes in ice thickness $\frac{\partial h}{\partial t}$ (red) are expressed in cm/day and all fluxes F (orange) are expressed in Wm^{-2}. F_{hor} is the sum of vertically-integrated temperature tendencies from horizontal diffusion and advection. F_{cb} and F_{ct} are the conduction fluxes at the bottom and the top of the ice. All other variable names are defined in section 2.2.

sion in Section 3.2). The basal and surface melt in the CESM-LE in the early 2000s (start of the transition to a seasonally ice free Arctic) are in general agreement with observations from post-2000 Ice Mass Balance buoys in the Beaufort Sea (97.64 ± 7.95 cm vs 61.92 ± 6.73 cm in the CESM-LE and 106 cm vs 62 cm in observations, Perovich & Richter-Menge, 2015). Changes in sea ice volume due to dynamical process (−1.96±7.09 cm) are again negligible compared to thermodynamic processes.

In February, the first order balance in the 1970-1979 ice-ocean heat budget is between the latent heat associated with freezing (18.15±1.12 W m^{-2}, or 14.35±0.88 cm of ice growth) and the conductive heat flux at the bottom of the ice ($F_{cb} = -18.30 \pm 1.10$ W m^{-2}). The small difference between latent and conductive heat flux is indicative of the small contribution from turbulent ice-ocean heat flux. The thermodynamic and dynamic ice growth, integrated over the full winter is equal to 35±9 cm in the 2.47 – 4.57 m ice thickness category (or 115.21±5.46 cm in all thickness categories) is in agreement with observations of 57 cm (including only the thermodynamic tendency, Untersteiner, 1961). The ice growth in the second thickest ice category is used in accord with mean ice thickness measurements in the Canada Basin. Looking at thinner ice would be biased to faster growth compared to thick ice floes where instruments are installed.

The second order balance in February heat budget is between the ice-atmosphere sensible heat flux through the leads ($F_{sens} = -1.59 \pm 0.16\ Wm^{-2}$), the latent heat flux associated with frazil ice formation ($F_{frazil} = 1.08 \pm 0.12\ Wm^{-2}$), lateral ocean heat transport ($F_{hor} = 1.36 \pm 0.63\ Wm^{-2}$), and change in internal energy ($\frac{\partial E}{\partial t} = -0.31 \pm 0.46\ Wm^{-2}$). Each term is nearly of the same order of magnitude as the residual error in the net heat budget ($-0.22 \pm 0.52 Wm^{-2}$).

Between 1970-1979 and 2010-2019 time periods, the basal growth is larger by 20% due to a decrease in ice/snow thickness and despite the reduced temperature gradient between the surface and ice base (ie. the negative ice growth-ice thickness feedback). However, the increased growth in the winter does not compensate for the 60% (87%) increase in basal (surface) melt. In the 2010-2019 time period, the ice growth integrated over the winter for the 2.47 – 4.57 m thickness category is equal to 57±13 cm (or 136.29±7.92 cm over all ice thickness categories) is in accord observations (59 cm, Perovich, D. et al., 2021). At the same time, the horizontal flux and the ice-ocean turbulent flux stayed nearly constant .

The fluxes calculated in this bulk ice-ocean budget will be used in the first layer of R (see eq. 5) in the 1D vertical heat budget. Figure 5 shows the complete seasonality of surface flux. The summer is dominated by the shortwave flux. In the fall, the heat is mostly leaving the surface by sensible and longwave flux over open water. In the winter, the most important flux is the sensible flux over leads, while the ice-ocean turbulent flux remains small. Hence, the heat stored in the ocean and ventilated in the winter is mostly use to impede the growth of new ice in leads rather than basal growth of exsiting ice.

3.2 Vertical T-S Profiles: CESM-LE vs Observations

Heat in the Canada Basin comes from three different sources located at different depths: the Near Surface Temperature Maximum (NSTM), the Pacific Waters (PW), and the Atlantic Waters (AW) (see figure 6).

From the 1970s to the early 2000s, observations indicate that the three September temperature maxima (NSTM, PW, AW) in the Canada Basin warmed by 0.09°C, 0.22°C, and 0.39°C, respectively (see Figure 6a). The surface ocean also became more stably stratified, with a reduction in the mixed-layer depth of 8 m and a reduction of sea surface salinity of 2.3 psu, as in (Rosenblum, Stroeve, et al., 2021). We also find that the winter PW (the second bump in the PW shaded area) is more visible in the early 2000s than in the mid-1970s; Whether this is due to sampling or warming is not clear.

By contrast, the CESM-LE shows very little change between 1970-1979 and 2010-2019 (Figure 6b). The temperature is nearly unchanged over the top 400 m, with the NSTM only warming by 0.06 °C. Similarly, the stratification is nearly the same, with only a 0.6 psu average change in salinity over the top 400 m, as in (Rosenblum, Fajber, et al., 2021).

Perhaps the most striking difference between the model and the observations is the complete absence of PW in the CESM-LE between 50 m and 100 m (see figure 6 c and d). This bias is likely related to an unrealistic PW pathway through through the Arc-

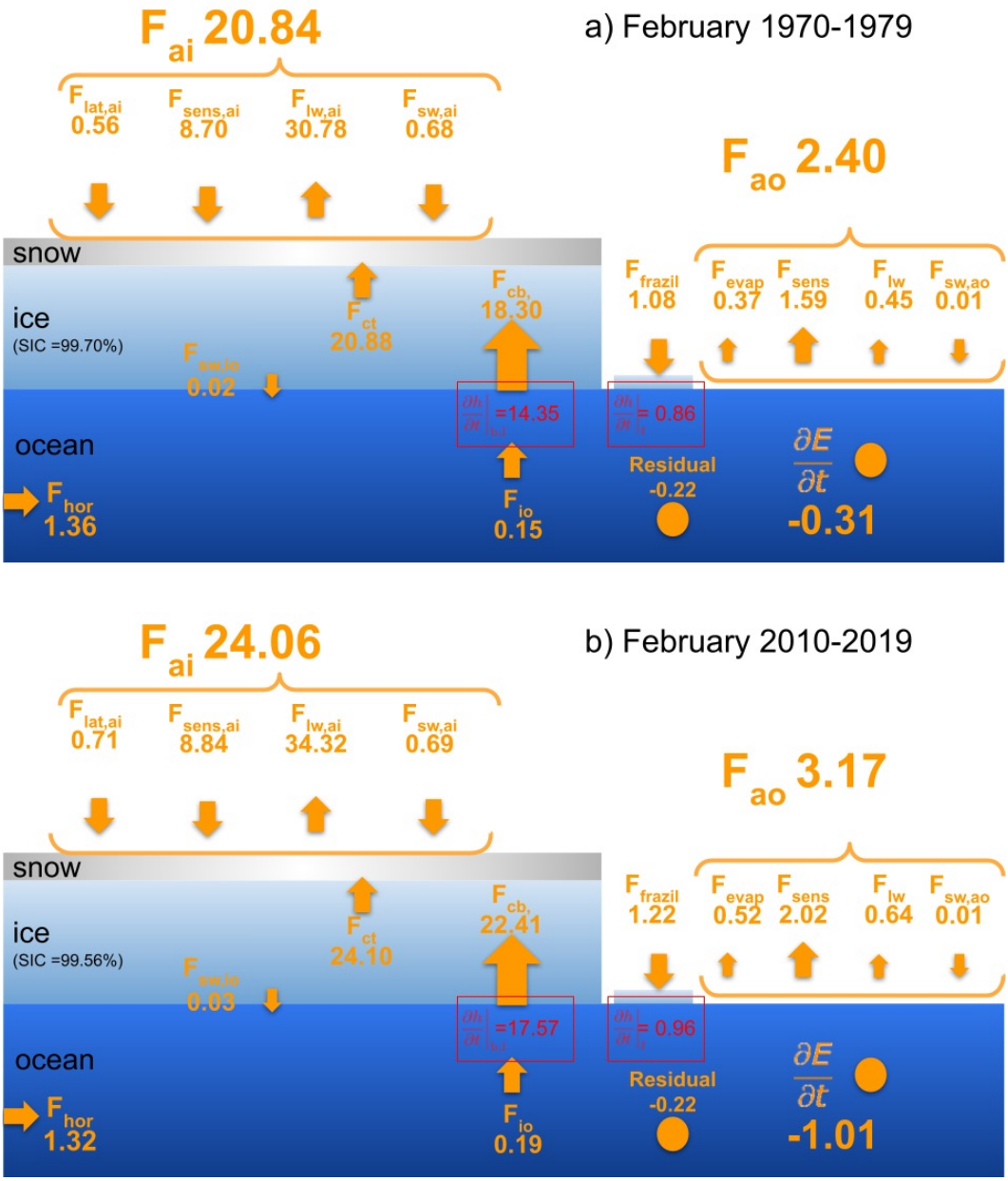

Figure 4. CESM-LE ensemble monthly mean heat budget for February averaged spatially over the Canada Basin and temporally over the years a) 1970-1979 and b) 2010-2019. Change in ice thickness $\frac{\partial h}{\partial t}$ (red) are expressed in cm/day. All fluxes F (orange) are expressed in Wm^{-2}. F_{hor} is the sum of vertically-integrated temperature tendencies from horizontal diffusion and advection. F_{cb} and F_{ct} are the conduction fluxes at the bottom and the top of the ice. All other variable names are defined in section 2.2.

tic, as in CCSM3 (an earlier version of the CESM-LE) (Jahn et al., 2010). Specifically, they found that the eastern PW branch does not penetrate far east and instead is entrained in a clockwise direction following the surface Beaufort Gyre around Point Barrow. The CESM probably has similar pathways as its predecessor since CCSM3 dye tracer results are in accord with the spacial distribution of silicate - a tracer used to track PW simulated by the CESM-LE (see figure 7). In-situ observation of silicates instead sug-

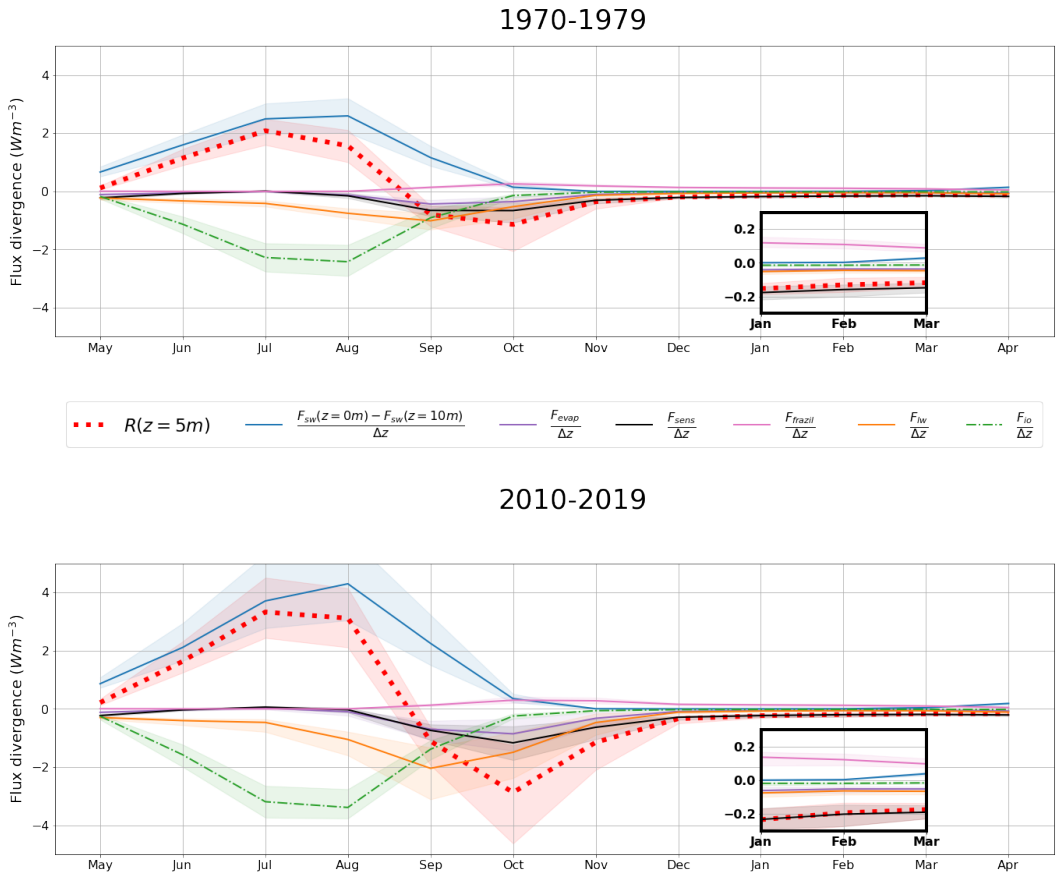

Figure 5. Simulated monthly divergence of fluxes in the top layer of the ocean in (top) 1970-1979 and (bottom) 2010-2019. The figure shows the divergence of the turbulent ice-ocean flux (part of D) and all the components of R in the top layer (at $z = z_1 = 5$ m) (see eq. 5). The shaded region represents the basin-average maximum/minimum over the 40 ensemble members.

gests that there is a large amount of PW in the Canada Basin entering directly from the Bering Strait over the Chukchi sea sea or via eddies breaking off the Alaskan Coastal Current (Pickart et al., 2005; Weingartner et al., 2005; Ladd et al., 2016).

Overall, the observed transition to a warmer more stratified Canada Basin from the 1970s to the early 2000s is missing in the CESM-LE. In the observations, there is a large freshening of the surface water for all months and a clear reduction of the May MLD (Figure 8 a and c; as in Peralta-Ferriz and Woodgate (2015); Rosenblum, Stroeve, et al. (2021)). Yet, in the CESM-LE, there is only a small freshening of the surface water and the winter mixed layer thickens instead (see figure 8 b and d). We note that the May MLD is well-represented in the CESM-LE in the 1970s, but fails to respond to the freshwater flux associated with sea ice thinning in the early 2000s (see figure 9). These findings are consistent with Rosenblum, Fajber, et al. (2021), who show that the model bias can be partly attributed to unrealistic vertical mixing, rather than sea ice melt. It appears that the net effect of increased melt and surface mixing by surface stress causes a more stable stratification in the observations and a less stable stratification in the CESM-LE. That is, the competition between wind-driven surface stress and fresh water input created by the recent large ice melting is won by fresh water input with increased stratification in observations (Peralta-Ferriz & Woodgate, 2015), and by increased surface stress

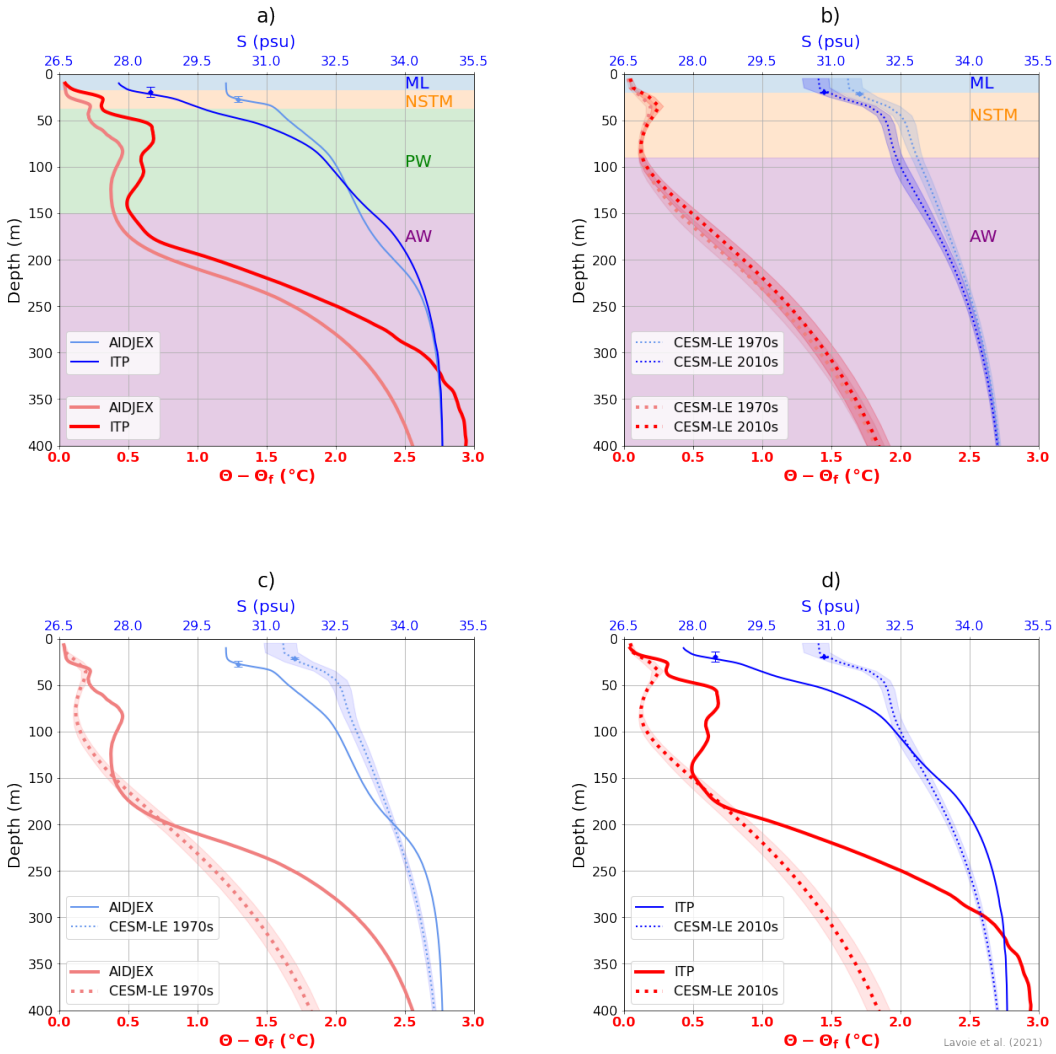

Figure 6. Observed and simulated September potential temperature anomaly from freezing (blue) and salinity (red) averaged over the Canada Basin in 1970-1979 and 2010-2019. a) Observations from 1975-76 (AIDJEX) and 2004-2018 (ITP), b) CESM-LE ensemble mean from 1970-1979 and 2010-2019, c) AIDJEX and CESM-LE 1970-1979, d) ITP and CESM-LE 2010-2019. (a,b) The Mixed Layer (ML), Near-Surface Temperature Maximum (NSTM), Pacific Water (PW), and Atlantic Water (AW) are indicated by blue, yellow, green, and purple shadings, respectively. The diamonds and error bars indicate the averaged mixed layer depths and standard deviations. The shaded region represents the maximum/minimum basin-average over the 40 ensemble members.

in the CESM-LE. This difference in stratification will have a large impact on vertical mixing between the mixed layer and the heat at depth (Toole et al., 2010).

The reduction of the mixed layer depth has repercussions on the ventilation of the NSTM. In 1975-1976 (AIDJEX), the observations indicate that the NSTM is only completely ventilated in May (see figure 8a). In 2004-2018, the observations (ITP) indicate that the NSTM has disappeared by December (Figure 8c). Whether it was ventilated to the surface or it merged with summer PW just beneath remains unclear. When looking at individual profiles, there is large spatial and/or time variability: In the 1970s, the

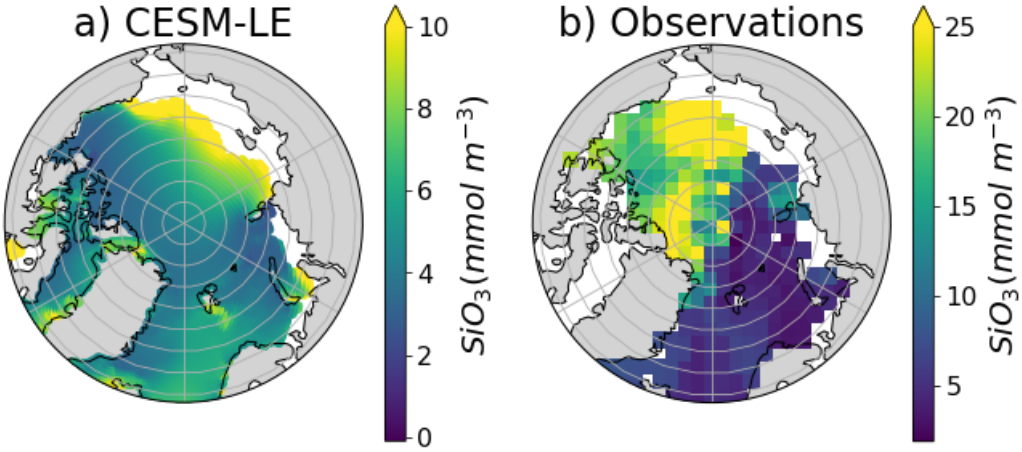

Figure 7. (a) Simulated and (b) observed summer (JAS) mean dissolved inorganic silicate average at 75m depth between 1948 and 2000 using the CESM ensemble mean and observations come from the World Ocean Atlas (Boyer et al., 2018). White space represents the shelf, which is shallower than 75m.

NSTM is absent from spring 1975, but clearly present in spring 1976 for the Caribou and BlueFox camps (see figure 10). This is presumably due to the fact that the camps started far north (high SIC) and drifted south (low SIC), where the open waters create better conditions for the creation of a warm NSTM. In the 2000s, the NSTM disappears between January (or earlier) and April (see ITP 41,75,53,82 in figure 11). Despite the large spatial/temporal variability, the NSTM in ITP data is less well-defined in the fall/winter and is ventilated more quickly than in AIDJEX presumably due to the more mobile thinner pack ice in the fall. In the CESM-LE, the ventilation of the NSTM lasts until May in both the 1970s and the 2000s, again missing a key transformation between the two time periods (figure 8b and d).

3.3 1D Heat Budget: Vertical Transport

We examine the CESM-LE basin-average change of heat at each depth ($\frac{\partial E}{\partial t}$) in response to three processes (equation 3): divergence of surface fluxes R, vertical diffusion D, and vertical advection $-\frac{\partial(Ew)}{\partial z}$ (see figure 12). In the following, the focus is on the 2000s when the same processes are observed and are more apparent than in the 1970s.

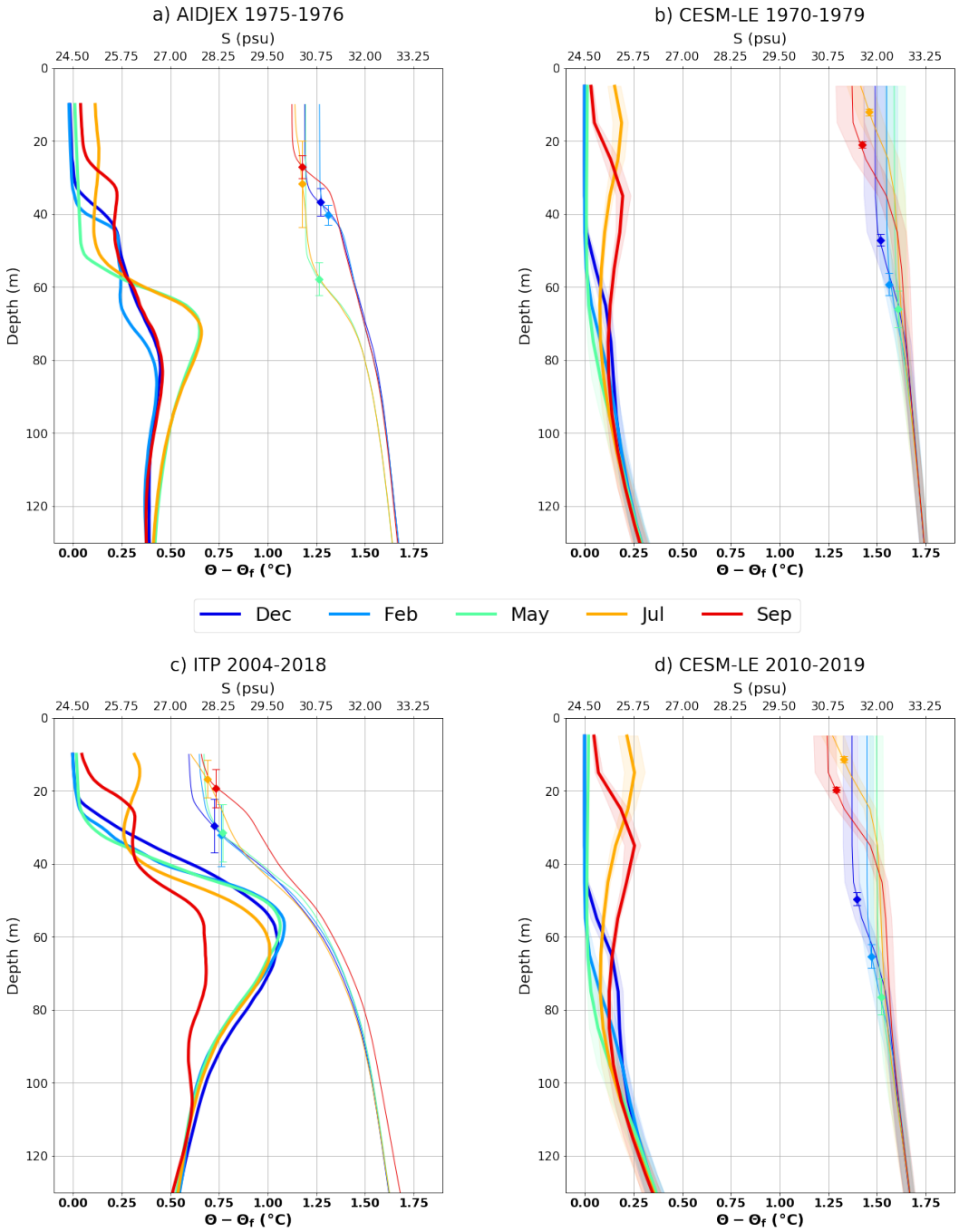

Figure 8. Observed and simulated monthly-mean, basin-average profiles of potential temperature anomaly from freezing (thick lines on the left) and salinity (thin lines on the right) using observations from (a) 1975-76 (AIDJEX) and (c) 2004-2018 (ITP), and the CESM-LE ensemble mean averaged over (b) 1970-1979 and (d) 2010-2019. The diamonds and error bars indicate the averaged mixed layer depth and the standard deviation. The shaded region indicates the basin-average maximum/minimum over the 40 ensemble members.

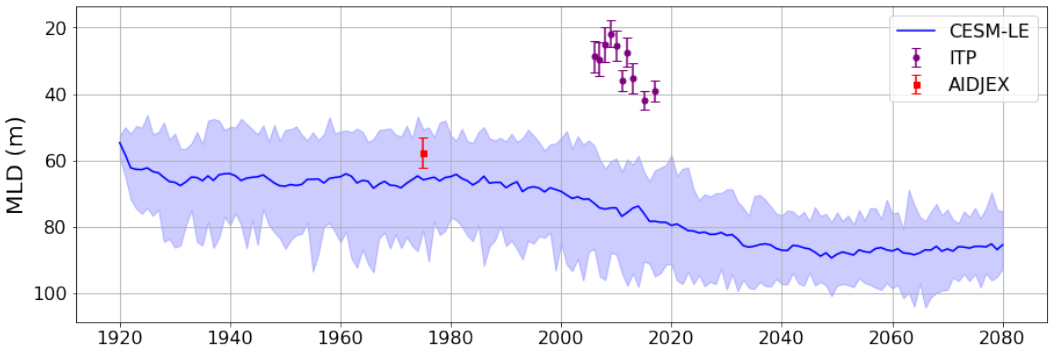

Figure 9. Observed and simulated May mixed layer depth (MLD) averaged over the Canada Basin between 1920 to 2080. The solid line indicates the ensemble mean and the shaded region indicates the basin-average minimum/maximum range over the 40 ensemble members. The purple round/red square markers indicate the observed mean and standard deviation of mixed layer depth from 1975-76 (AIDJEX) and 2004-2018 (ITP).

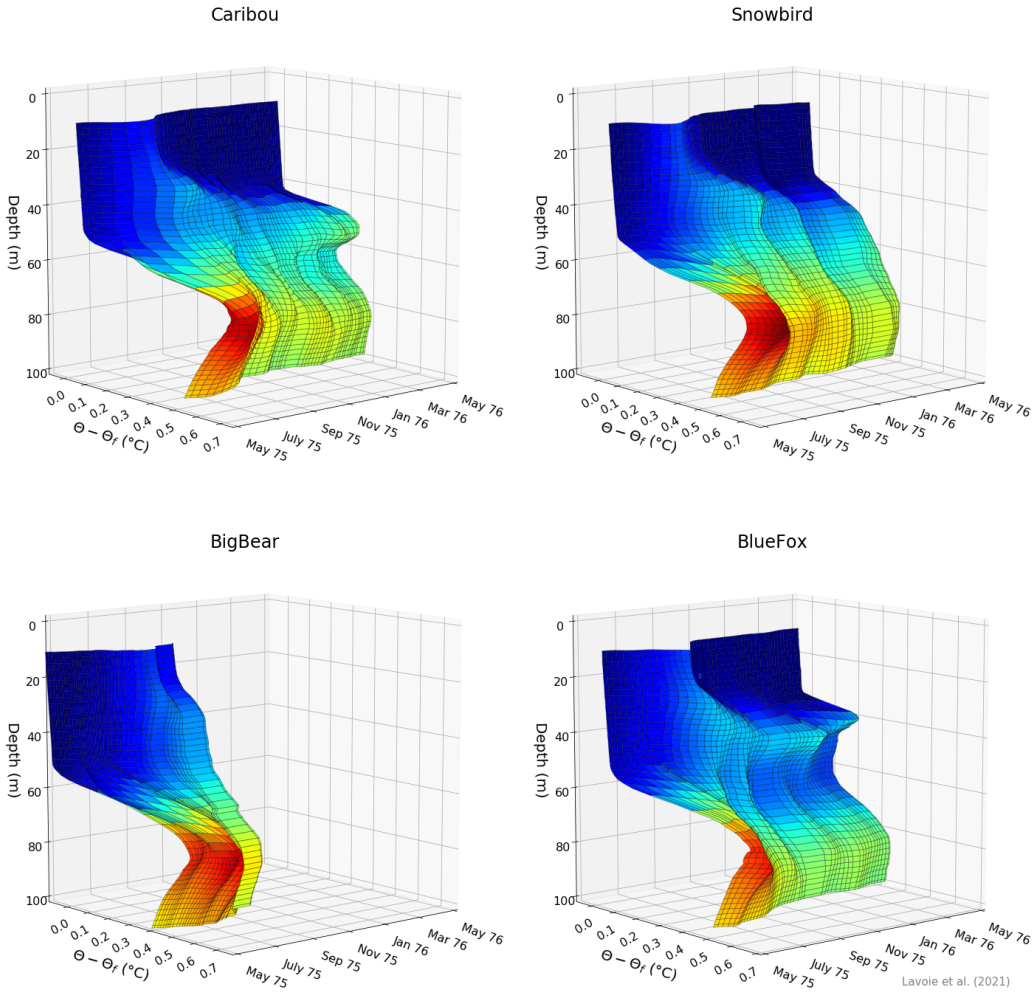

Figure 10. Observed seasonal evolution of the potential temperature anomaly from freezing profiles for the four 1975-1976 AIDJEX camps. The profiles have been smoothed in time with a Gaussian filter. Figure inspired by Maykut and McPhee (1995).

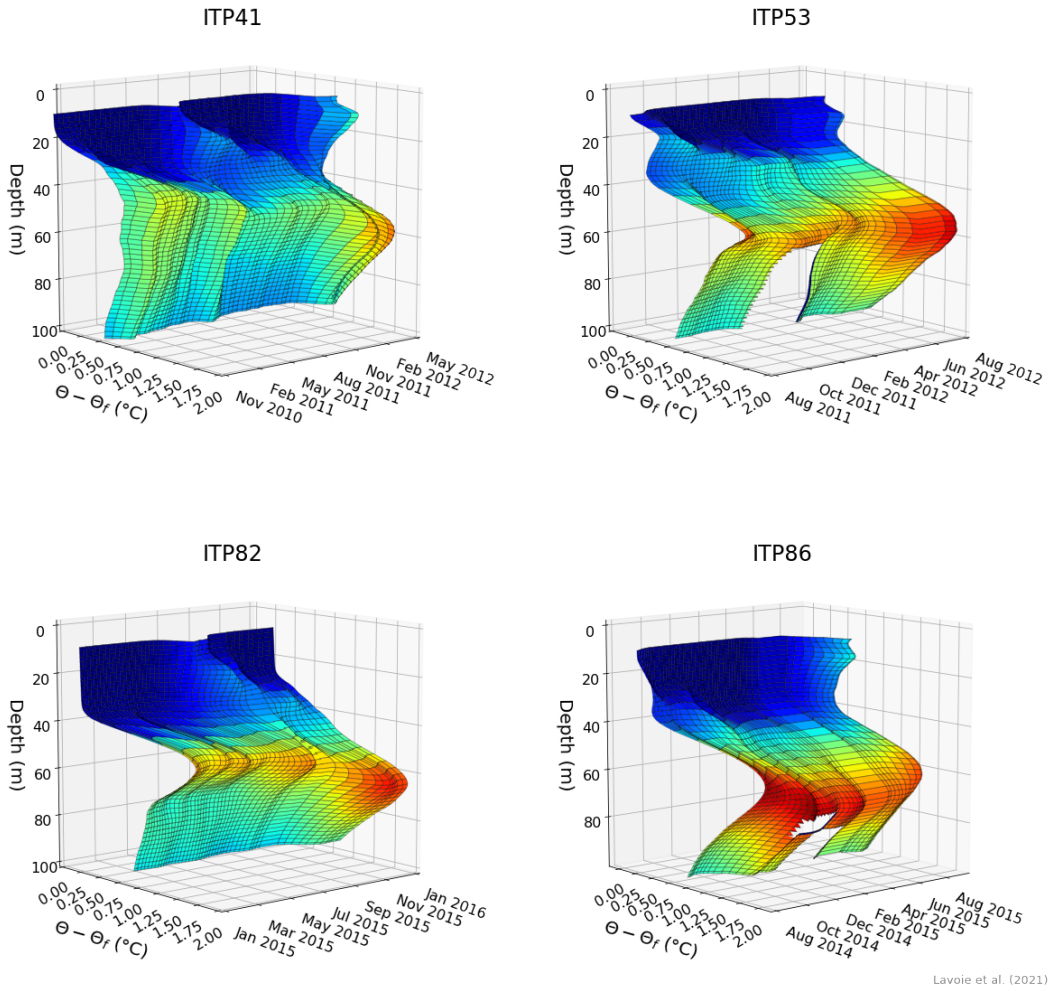

Figure 11. Observed seasonal evolution of the potential temperature anomaly from freezing profiles for four representatives (out of 36) ITPs. The profiles have been smoothed in time with a Gaussian filter. Note that the time axis is different for each subplot. Figure inspired by Maykut and McPhee (1995).

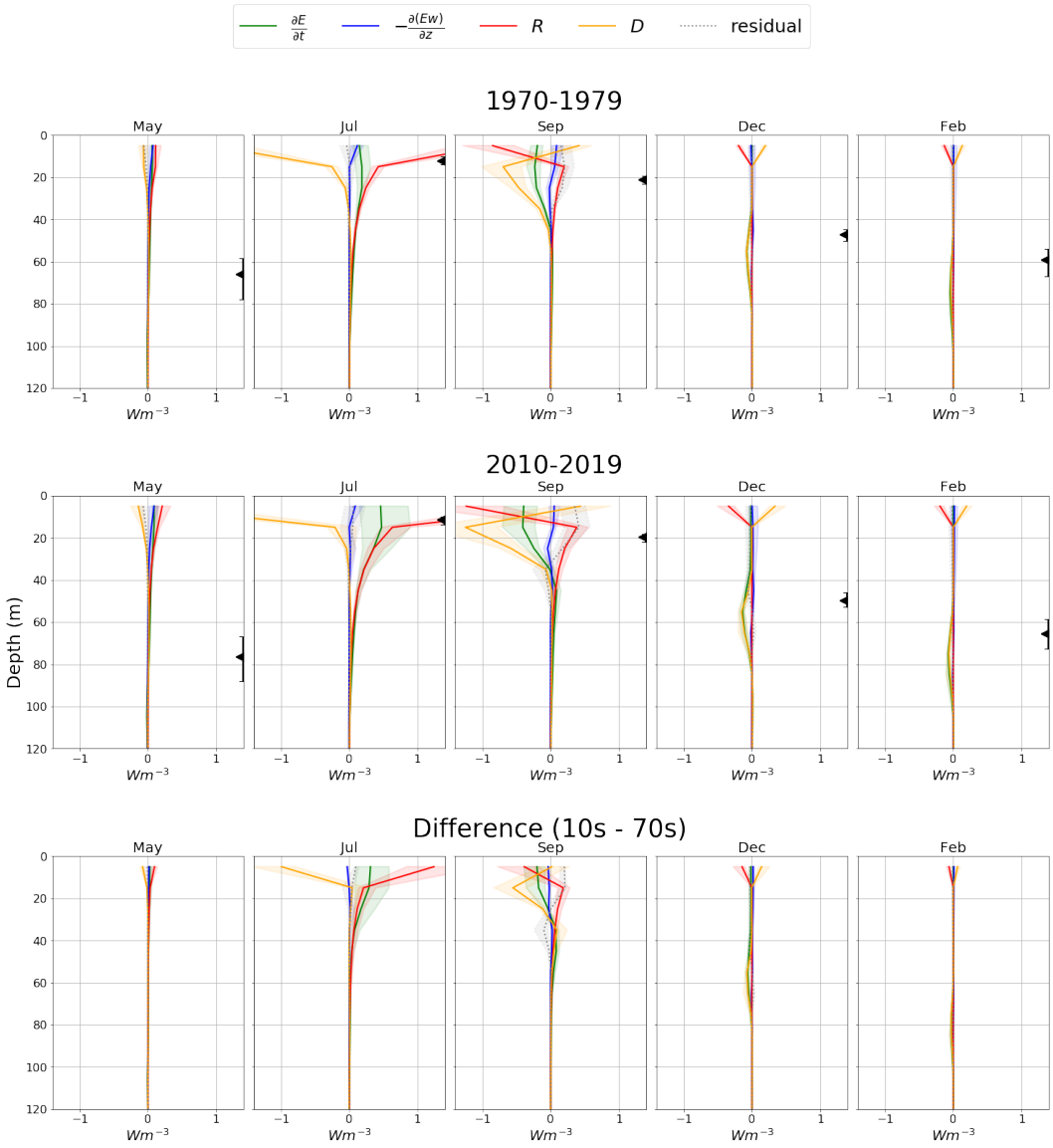

Figure 12. Estimated monthly vertical ocean heat budget using CESM-LE simulations of 1970-1979 (top), 2010-2019 (center), and their difference (bottom). The change in internal energy (green), divergence of surface fluxes (red), vertical diffusion (orange), vertical advection (blue), and the residual error (dotted grey) are indicated (see eq. 3 for details). The shaded region represents the basin-average maximum/minimum over the 40 ensemble members. Black trianges and errorbars indicate the basin-average mixed-layer depth and its maximum/minimum range. Note that the data for July exceeds the horizontal scale at 5 m in order to resolve fine-scale features in the winter. A positive value indicates that the process acts to increase heat and a negative value indicates that the process acts to decrease heat at a given depth.

In the summer, the main balance is between the divergence of the surface fluxes (R), dominated by the shorthwave flux, and the turbulent mixing (D), with the change in internal energy as a second order term ($\frac{\partial E}{\partial t}$). In early summer, the SIC is high and surface fluxes entering the mixed layer leads to ice melt via ice-ocean turbulent at flux. Less importantly, heat from the NSTM is diffused upward to the surface by diffusion.

In the fall, this balance reverses and heat stored below the surface ($\frac{\partial E}{\partial t}$) is brought up to the surface by diffusion (D) and lost to the atmosphere by surface fluxes (R), mostly sensible and longwave. In late summer and early fall, the change in internal energy are large as the sea ice concentration is much lower. At depth, some heat is gained through penetrating shortwave (R) until about 40 m.

From November to April, the heat stored in the NSTM is ventilated – matching negative peaks in $\frac{\partial E}{\partial t}$ and D that decreases in amplitude and increases in depth – with convection induced by salt rejection that erodes the seasonal halocline and deepens the mixed layer. The heat brought up by diffusion leaves the ocean through surface fluxes (R), mainly with the sensible flux through leads. There is no solar flux in winter, hence there is no surface flux below the first layer of the ocean.

Vertical heat flux associated with Ekman pumping downward ($\sim$1 myr^{-1} to 20 myr^{-1}) is highest in the fall when the winds are strong and the pack still relatively open and weak (Meneghello, Marshall, Timmermans, & Scott, 2018; Petty et al., 2016), but even then, is relatively small compared with other terms in the budget. The near zero advection term in the winter is also consistent with the weakening of the anticylonic ice drift associated with thick ice (Meneghello, Marshall, Timmermans, & Scott, 2018).

We next show the decomposition of the diffusion flux in figure 13. In the summer, diabatic diffusion brings a little bit of heat from the halocline to the top layer. The ice-ocean turbulent flux transfers the heat from the top layer, mostly brought by shortwave flux, to the ice. In the fall, both diabatic and non-local diffusion remove heat from the halocline to bring it to the surface. In the winter, the ventilation of the NSTM is characterized by a double peak in diabatic diffusion that move heat upward and downward (the downward peak is not visible on this scale, see figure 13, cyan line). This heat brought upward reaches the bottom of the mixed layer where the non-local diffusion takes it to the surface.

To confirm our 1D assumption in the vertical heat budget, we calculate the residual and the portion of the residual of the 1D budget that is due to heat transport from horizontal processes (see figure 14). The budget has a very small residual from November to August. In the summer, the residual is quite small and can be mostly explained by horizontal heat fluxes. In the fall, the residual is larger, because there are larger temporal and spatial changes in internal heat leading to more error from the time discretization of the energy tendency term.

The vertical migration of heat is similar in 1970-1979 and 2010-2019, with larger heat fluxes in recent years (see the bottom row of figure 12). In July, there is more solar heat penetrating the ocean and, therefore, more heat stored in the ocean and more turbulent ice-ocean flux. However, the vertical diffusion of heat remains constant, similar to the vertical distribution of freshwater (Rosenblum, Fajber, et al., 2021). The input of heat to the ocean, through shortwave flux, increases, but the diffusion stays nearly the same. Hence, more heat is accumulated in the column. This extra heat will only be ventilated later in the year. There is more heat diffused upward from the halocline to the surface in 2010-2019 than in 1970-1979. This indicates that the extra heat accumulated in the ocean in recent years is mainly ventilated in the fall and winter.

The simulated biases related to the NSTM and PW will impact the vertical transport of heat in the ocean and the sea ice mass balance. The 2010-2019 NSTM is unrealistically cold and deep, implying that less heat will reach the surface. Further, the missing Pacific Water implies a missing vertical ocean heat flux that would lead to reduce ice formation in winter. The temperature gradient induced by the presence of Pacific Waters is similar or greater than the one associated with the NSTM (see figure 8). This provides a low bound estimate of the ocean heat flux from the vertical mixing of Pacific Waters in the CESM-LE (0.62 W m^{-3} for a 10 m layer thickness, the average heat brought to the top layer by diffusion), equivalent to 1.4 m of reduced winter ice growth over 3 years, the residence time in the Canada Basin (G.G. Campbell et al., 2021). In the summer, the warm Pacific Waters are well below the seasonal pycnocline and are not believed to have a significant impact on the summer ice melt. This estimate is in the same or-

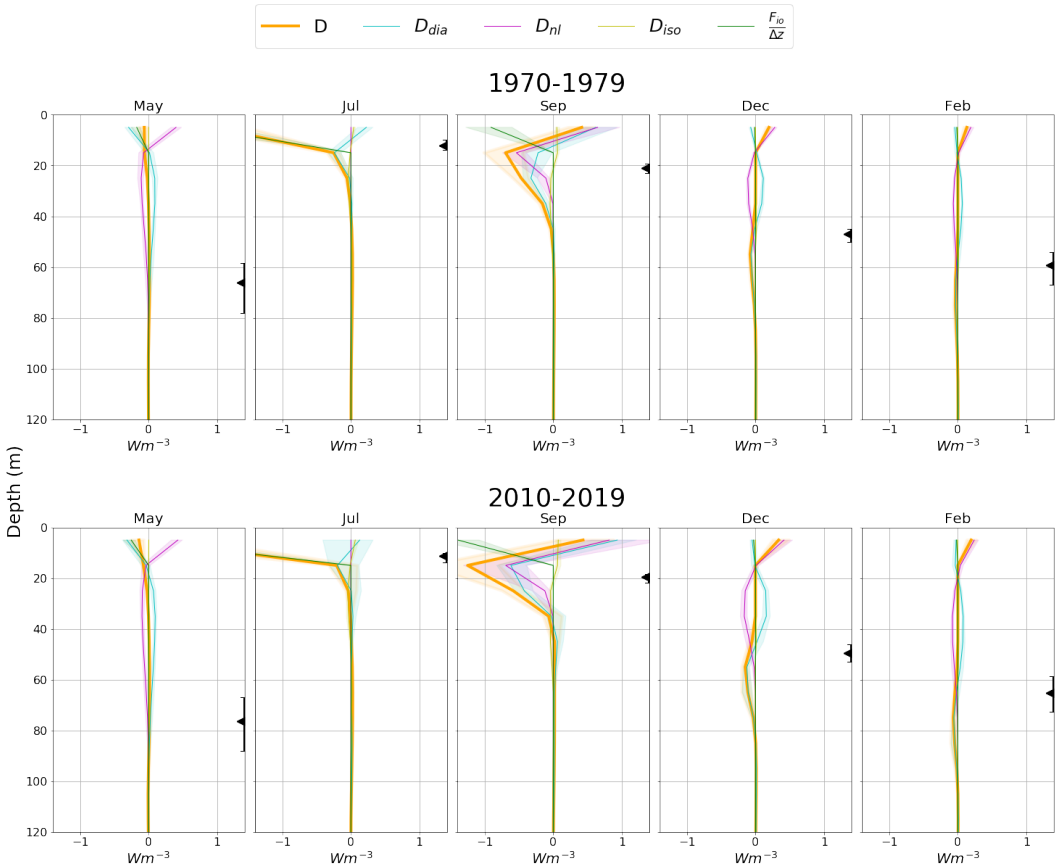

Figure 13. Simulated monthly change in heat from diffusive processes in 1970-1979 (top) and 2010-2019 (bottom). The total diffusion of heat (orange) occurs in response to the sum of the four processes: diabatic diffusion (cyan), non-local processes (pink), isopycnal diffusion (yellow), and ice-ocean turbulent heat flux (green). The shaded region represents the basin-average maximum/minimum over the 40 ensemble members.

der of magnitude as the 1.75 m of melt between 1980 and 2008 found by Kwok and Rothrock (2009). Future work will be focused on a more precise estimation and will be calculated using a 1D column model of the vertical heat and salt transport constrained by observed vertical temperature and salinity profiles.

4 Conclusions

We quantified changes to the seasonal vertical ice-ocean heat budget and sea ice mass balance between 1970-1979 and 2010-2019 in the Canada Basin using simulations from the CESM-LE. By examining the simulated transition from a seasonal to a perennial ice cover (pre and post-2000) and comparing with observations from 2004-2018 ITPs and 1975-1976 AIDJEX ice camps, we assess the reality of the simulated ocean heat transport.

First, we show that the summer ice-ocean heat budget is mainly balanced by the net shortwave radiation, the turbulent ice-ocean heat flux, and the internal heat change in the ocean. Compared to 1970-1979, the 2010-2019 ice-ocean turbulent flux and solar heat flux was ∼40% larger, contributing to a basal melt that was ∼60% larger. The net

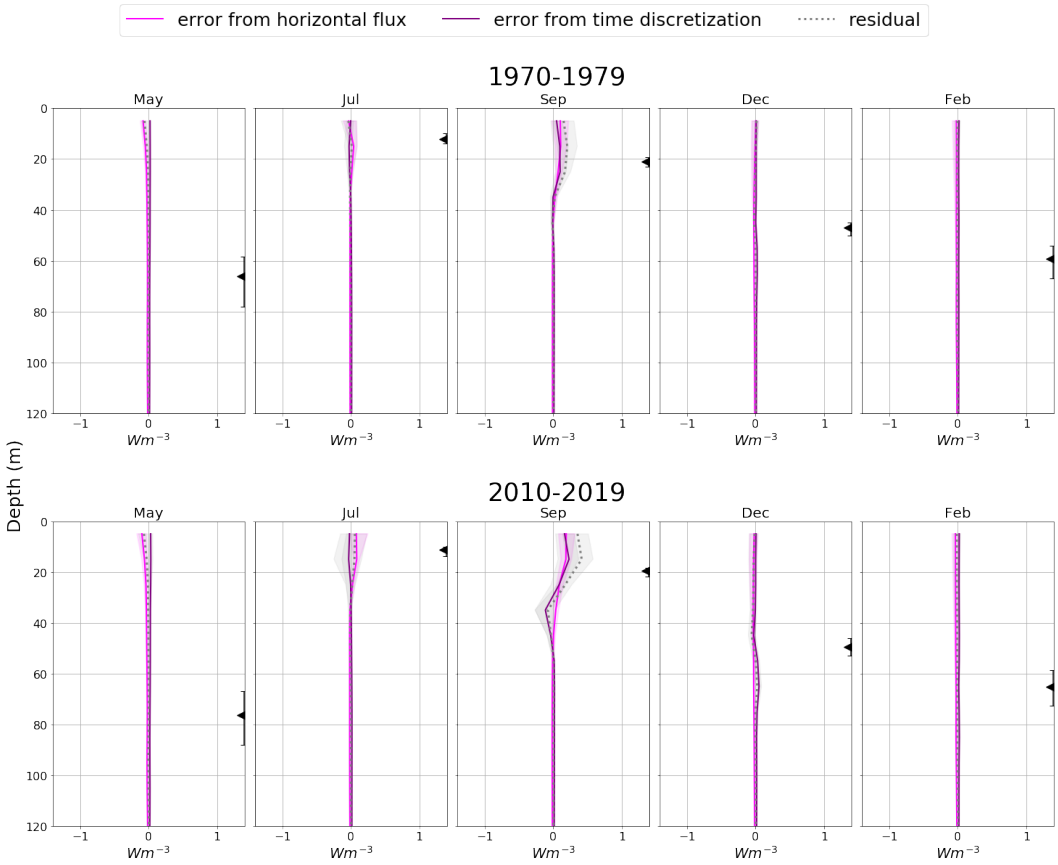

Figure 14. Simulated monthly decomposition of the residual in 1970-1979 (top) and 2010-2019 (bottom). This figure reproduces the residual from figure 12 (dotted grey line) and shows the part of the error that comes from heat tendency from horizontal flux (advection and diffusion) (pink). The error from the second order scheme of the energy time derivative (purple) is calculated as the difference between the residual and the horizontal contribution. The shaded region represents the maximum/minimum over the 40 ensemble members.

decrease in ice thickness was more moderate because of the increased in basal growth of 20% (the negative ice thickness – ice growth feedback).

Second, we found two main discrepancies between the model and the observations. The most striking difference is the complete absence of heat from Pacific Water in CESM-LE. By examining silicates, a tracer of Pacific Waters, we confirmed that the model incorrectly simulates the transport of Pacific Water into the Canada Basin. Instead, simulated PW follows the Alaskan coastline and is mostly entrained anticyclonically with the surface waters around Point Barrow. This is consistent with Zhang and Steele (2007), who showed that larger vertical diffusion increases the vertical extent of the surface anticyclonic circulation at the expense of the cyclonic at depth. The second large discrepancy – in opposition with observations showing an increased vertical stratification associated with ice melt as found by Peralta-Ferriz and Woodgate (2015) – is the increase in vertical mixing associated with a more mobile thinner pack ice despite increased surface freshwater fluxes associated with sea ice melt. This opposite process dominates in the CESM-LE, as the mixed layer depth is correctly represented in the 1970s but increases instead of decreasing as observed (Rosenblum, Stroeve, et al., 2021). Again, this points to a problem in vertical mixing of the CESM-LE, consistent with previous studies (Holloway

et al., 2007; Ilıcak et al., 2016; Rosenblum, Fajber, et al., 2021). Another change between the two periods that is not properly reproduced in the CESM-LE is the ventilation of the NSTM. In general, the NSTM has disappeared by May in the AIDJEX data and by December in the ITP data, but the CESM-LE shows an NSTM until May in both periods. We noted that there is large spatial and time variability by looking at individual AIDJEX camps and ITPs.

Third, a 1D budget of the vertical heat transport was presented. In general, the heat tendency from surface fluxes R is mirrored by the turbulent diffusion D. The vertical advection term is small compared to the other terms, even in the fall when the winds are strong and the pack-ice is still unconsolidated and mobile. This balance breaks down in the fall when the internal energy tendency term changes rapidly, which creates a larger error with the second-order differentiation scheme. In the summer, penetrating shortwave radiation warms the water column down to 80 m. Diabatic diffusion then takes heat in the seasonal halocline and brings it back to the surface, melting the ice. In the fall, diabatic diffusion takes heat accumulated in the mixed layer to the surface where it leaves through mostly sensible and longwave fluxes. In the winter, there is some remnant solar heat from the summer stored in the winter halocline. The diabatic diffusion brings it up to the bottom of the deep mixed layer and the non-local diffusion lifts it up to the surface where most of the heat leaves through the leads by sensible flux. Hence, the winter ocean remnant heat does not impede basal growth greatly, but stops new ice from forming in the leads. This balance does not go through large changes from the 1970s to the early 2000s. The amplitudes of all heat terms just get larger. Using this budget, a rough estimation was made that the missing Pacific Waters heat source would create ∼1.4 m of reduced winter ice growth over 3 years, a significant contribution, though a 1d model would be necessary to make a more accurate estimate. This will be the subject of future work.

Acknowledgments

All model output variables are available on the NCAR Climate Data Gateway at `https://www.cesm.ucar.edu/projects/community-projects/LENS/data-sets.html`.The Ice-Tethered Profiler data were collected and made available by the Ice-Tethered Profiler Program based at the Woods Hole Oceanographic Institution (`http://www.whoi.edu/itp`). The AIDJEX data is available at `http://lwbin-datahub.ad.umanitoba.ca/dataset/aidjex`. The code for the analysis is available on Juliette Lavoie's github page `https://github.com/juliettelavoie/verticalHeat` and Zenodo `https://zenodo.org/account/settings/github/repository/juliettelavoie/verticalHeat#` associated with `DOI: 10.5281/zenodo.5041484`.

Juliette Lavoie would like to thank the Fonds de recherche du Québec - Nature et technologies (FRQNT) for the Bourse de maîtrise en recherche and the Natural Sciences and Engineering Research Council of Canada (NSERC) for the Canada Graduate Scholarships-Master's (CGS M). She is also grateful for the support of McGill University, Québec-Océan and Arctrain Canada. This project a contribution to the the Natural Science and Engineering Research Council - Discovery Program and the NASA grant #80NSSC20K1259 entitled, The role of midlatitude cyclones in the seasonal evolution of the coupled atmosphere-sea ice-ocean system in the Labrador Sea and the Greenland Sea and the NSF Office of Polar Program grant # 1504023, #1603350 and #1928126. Finally, we would like to acknowledge the CESM Large Ensemble Community Project and supercomputing resources provided by NSF/CISL/Yellowstone. Erica Rosenblum was supported by the National Sciences and Engineering Research Council of Canada (NSERC) PDF award. We would also like to acknowledge Dr David Straub from McGill University for his useful comments.

References

Aagaard, K., Coachman, L., & Carmack, E. (1981, June). On the halocline of the

Arctic Ocean. *Deep Sea Research Part A. Oceanographic Research Papers*, *28*(6), 529–545. Retrieved 2020-09-25, from https://linkinghub.elsevier.com/retrieve/pii/0198014981901151 doi: 10.1016/0198-0149(81)90115-1

Auclair, G., & Tremblay, L. B. (2018). The Role of Ocean Heat Transport in Rapid Sea Ice Declines in the Community Earth System Model Large Ensemble. *Journal of Geophysical Research: Oceans*, *123*(12), 8941–8957. Retrieved 2020-09-24, from https://agupubs.onlinelibrary.wiley.com/doi/abs/10.1029/2018JC014525 (_eprint: https://agupubs.onlinelibrary.wiley.com/doi/pdf/10.1029/2018JC014525) doi: 10.1029/2018JC014525

Bitz, C. M., Holland, M. M., Weaver, A. J., & Eby, M. (2001). Simulating the ice-thickness distribution in a coupled climate model. *Journal of Geophysical Research: Oceans*, *106*(C2), 2441–2463. Retrieved 2021-06-10, from https://agupubs.onlinelibrary.wiley.com/doi/abs/10.1029/1999JC000113 (_eprint: https://agupubs.onlinelibrary.wiley.com/doi/pdf/10.1029/1999JC000113) doi: 10.1029/1999JC000113

Bitz, C. M., & Lipscomb, W. H. (1999). An energy-conserving thermodynamic model of sea ice. *Journal of Geophysical Research: Oceans*, *104*(C7), 15669–15677. Retrieved 2021-06-10, from https://agupubs.onlinelibrary.wiley.com/doi/abs/10.1029/1999JC900100 (_eprint: https://agupubs.onlinelibrary.wiley.com/doi/pdf/10.1029/1999JC900100) doi: 10.1029/1999JC900100

Boyer, T. P., Garcia, H. E., Locarnini, R. A., Zweng, M. M., Mishonov, A. V., Reagan, J. R., ... Smolyar, I. V. (2018). *World Ocean Atlas 2018.* Retrieved 2021-03-29, from http://www.ncei.noaa.gov/products/world-ocean-atlas

Carmack, E., Polyakov, I., Padman, L., Fer, I., Hunke, E., Hutchings, J., ... Winsor, P. (2015, December). Toward Quantifying the Increasing Role of Oceanic Heat in Sea Ice Loss in the New Arctic. *Bulletin of the American Meteorological Society*, *96*(12), 2079–2105. Retrieved 2020-11-06, from https://journals.ametsoc.org/bams/article/96/12/2079/69295/Toward-Quantifying-the-Increasing-Role-of-Oceanic (Publisher: American Meteorological Society) doi: 10.1175/BAMS-D-13-00177.1

Curry, J. (1999). *SHEBA ISFF Flux-PAM Project Report | Earth Observing Laboratory.* Retrieved 2021-05-10, from https://www.eol.ucar.edu/content/sheba-isff-flux-pam-project-report

Davis, P. E. D., Lique, C., & Johnson, H. L. (2014, November). On the Link between Arctic Sea Ice Decline and the Freshwater Content of the Beaufort Gyre: Insights from a Simple Process Model. *Journal of Climate*, *27*(21), 8170–8184. Retrieved 2021-01-12, from https://journals.ametsoc.org/view/journals/clim/27/21/jcli-d-14-00090.1.xml (Publisher: American Meteorological Society Section: Journal of Climate) doi: 10.1175/JCLI-D-14-00090.1

Davis, P. E. D., Lique, C., Johnson, H. L., & Guthrie, J. D. (2016, May). Competing Effects of Elevated Vertical Mixing and Increased Freshwater Input on the Stratification and Sea Ice Cover in a Changing Arctic Ocean. *Journal of Physical Oceanography*, *46*(5), 1531–1553. Retrieved 2020-09-23, from https://journals.ametsoc.org/jpo/article/46/5/1531/342929/Competing-Effects-of-Elevated-Vertical-Mixing-and doi: 10.1175/JPO-D-15-0174.1

DeRepentigny, P., Tremblay, L. B., Newton, R., & Pfirman, S. (2016, October). Patterns of Sea Ice Retreat in the Transition to a Seasonally Ice-Free Arctic. *Journal of Climate*, *29*(19), 6993–7008. Retrieved 2021-03-10, from https://journals.ametsoc.org/view/journals/clim/29/19/jcli-d-15-0733.1.xml (Publisher: American Meteorological Society Section: Journal of Climate) doi: 10.1175/JCLI-D-15-0733.1

Desmarais, A., & Tremblay, B. (2021, February). Assessment of decadal variability in sea ice in the Community Earth System Model against a long-term regional observational record: implications for the predictability of an ice-free Arctic. *Journal of Climate*, *-1*(aop). Retrieved 2021-03-10, from https://journals.ametsoc.org/view/journals/clim/aop/JCLI-D-20-0561.1/JCLI-D-20-0561.1.xml (Publisher: American Meteorological Society Section: Journal of Climate) doi: 10.1175/JCLI-D-20-0561.1

Fetterer, F., Knowles K., Meier W., Savoie M., & Windnagel A. (2017). *Sea Ice Index, Version 3.* NSIDC. Retrieved 2021-06-10, from https://nsidc.org/data/G02135/versions/3 (Type: dataset) doi: 10.7265/N5K072F8

Gent, P. R., & Mcwilliams, J. C. (1990, January). Isopycnal Mixing in Ocean Circulation Models. *Journal of Physical Oceanography*, *20*(1), 150–155. Retrieved 2021-06-10, from https://journals.ametsoc.org/view/journals/phoc/20/1/1520-0485_1990_020_0150_imiocm_2_0_co_2.xml (Publisher: American Meteorological Society Section: Journal of Physical Oceanography) doi: 10.1175/1520-0485(1990)020⟨0150:IMIOCM⟩2.0.CO;2

G.G. Campbell, S. Pfirman, B. Tremblay, R. Newton, W. Meier, & C. Fowler. (2021). *SITU | Sea Ice Tracking Utility. The Ice Tracker.* Retrieved 2021-05-20, from http://icemotion.labs.nsidc.org/SITU/

Gong, D., & Pickart, R. S. (2015, August). Summertime circulation in the eastern Chukchi Sea. *Deep Sea Research Part II: Topical Studies in Oceanography*, *118*, 18–31. Retrieved 2021-03-29, from https://www.sciencedirect.com/science/article/pii/S096706451500034X doi: 10.1016/j.dsr2.2015.02.006

Goosse, H., Deleersnijder, E., Fichefet, T., & England, M. H. (1999). Sensitivity of a global coupled ocean-sea ice model to the parameterization of vertical mixing. *Journal of Geophysical Research: Oceans*, *104*(C6), 13681–13695. Retrieved 2021-05-07, from https://agupubs.onlinelibrary.wiley.com/doi/abs/10.1029/1999JC900099 (_eprint: https://agupubs.onlinelibrary.wiley.com/doi/pdf/10.1029/1999JC900099) doi: https://doi.org/10.1029/1999JC900099

Holloway, G., Dupont, F., Golubeva, E., Häkkinen, S., Hunke, E., Jin, M., ... Zhang, J. (2007). Water properties and circulation in Arctic Ocean models. *Journal of Geophysical Research: Oceans*, *112*(C4). Retrieved 2021-02-04, from https://agupubs.onlinelibrary.wiley.com/doi/abs/10.1029/2006JC003642 (_eprint: https://agupubs.onlinelibrary.wiley.com/doi/pdf/10.1029/2006JC003642) doi: https://doi.org/10.1029/2006JC003642

Hunke, E. C., & Dukowicz, J. K. (1997, September). An Elastic–Viscous–Plastic Model for Sea Ice Dynamics. *Journal of Physical Oceanography*, *27*(9), 1849–1867. Retrieved 2021-06-10, from https://journals.ametsoc.org/view/journals/phoc/27/9/1520-0485_1997_027_1849_aevpmf_2.0.co_2.xml (Publisher: American Meteorological Society Section: Journal of Physical Oceanography) doi: 10.1175/1520-0485(1997)027⟨1849:AEVPMF⟩2.0.CO;2

Huwald, H., Tremblay, L.-B., & Blatter, H. (2005). Reconciling different observational data sets from Surface Heat Budget of the Arctic Ocean (SHEBA) for model validation purposes. *Journal of Geophysical Research: Oceans*, *110*(C5). Retrieved 2021-05-17, from https://agupubs.onlinelibrary.wiley.com/doi/abs/10.1029/2003JC002221 (_eprint: https://agupubs.onlinelibrary.wiley.com/doi/pdf/10.1029/2003JC002221) doi: https://doi.org/10.1029/2003JC002221

Iacono, M. J., Delamere, J. S., Mlawer, E. J., Shephard, M. W., Clough, S. A., & Collins, W. D. (2008). Radiative forcing by long-lived greenhouse gases: Calculations with the AER radiative transfer models. *Journal of Geophysical Research: Atmospheres*, *113*(D13). Retrieved 2021-06-10, from https://agupubs.onlinelibrary.wiley.com/doi/abs/10.1029/2008JD009944 (_eprint:

https://agupubs.onlinelibrary.wiley.com/doi/pdf/10.1029/2008JD009944) doi: 10.1029/2008JD009944

Ilıcak, M., Drange, H., Wang, Q., Gerdes, R., Aksenov, Y., Bailey, D., ... Yeager, S. G. (2016, April). An assessment of the Arctic Ocean in a suite of interannual CORE-II simulations. Part III: Hydrography and fluxes. *Ocean Modelling*, *100*, 141–161. Retrieved 2021-02-04, from https://www.sciencedirect.com/science/article/pii/S1463500316000238 doi: 10.1016/j.ocemod.2016.02.004

Jackson, J. M., Carmack, E. C., McLaughlin, F. A., Allen, S. E., & Ingram, R. G. (2010). Identification, characterization, and change of the near-surface temperature maximum in the Canada Basin, 1993–2008. *Journal of Geophysical Research: Oceans*, *115*(C5). Retrieved 2020-09-24, from https://agupubs.onlinelibrary.wiley.com/doi/abs/10.1029/2009JC005265 (_eprint: https://agupubs.onlinelibrary.wiley.com/doi/pdf/10.1029/2009JC005265) doi: 10.1029/2009JC005265

Jackson, J. M., Williams, W. J., & Carmack, E. C. (2012, February). Winter sea-ice melt in the Canada Basin, Arctic Ocean: WINTER SEA-ICE MELT CANADA BASIN. *Geophysical Research Letters*, *39*(3), n/a–n/a. Retrieved 2021-02-19, from http://doi.wiley.com/10.1029/2011GL050219 doi: 10.1029/2011GL050219

Jahn, A., Tremblay, L. B., Newton, R., Holland, M. M., Mysak, L. A., & Dmitrenko, I. A. (2010). A tracer study of the Arctic Ocean's liquid freshwater export variability. *Journal of Geophysical Research: Oceans*, *115*(C7). Retrieved 2020-09-24, from https://agupubs.onlinelibrary.wiley.com/doi/abs/10.1029/2009JC005873 (_eprint: https://agupubs.onlinelibrary.wiley.com/doi/pdf/10.1029/2009JC005873) doi: 10.1029/2009JC005873

Jones, E. P., Swift, J. H., Anderson, L. G., Lipizer, M., Civitarese, G., Falkner, K. K., ... McLaughlin, F. (2003). Tracing Pacific water in the North Atlantic Ocean. *Journal of Geophysical Research: Oceans*, *108*(C4). Retrieved 2021-03-06, from https://agupubs.onlinelibrary.wiley.com/doi/abs/10.1029/2001JC001141 (_eprint: https://agupubs.onlinelibrary.wiley.com/doi/pdf/10.1029/2001JC001141) doi: https://doi.org/10.1029/2001JC001141

Kay, J. E., Deser, C., Phillips, A., Mai, A., Hannay, C., Strand, G., ... Vertenstein, M. (2015, August). The Community Earth System Model (CESM) Large Ensemble Project: A Community Resource for Studying Climate Change in the Presence of Internal Climate Variability. *Bulletin of the American Meteorological Society*, *96*(8), 1333–1349. Retrieved 2021-05-04, from https://journals.ametsoc.org/view/journals/bams/96/8/bams-d-13-00255.1.xml (Publisher: American Meteorological Society Section: Bulletin of the American Meteorological Society) doi: 10.1175/BAMS-D-13-00255.1

Kim, R., Tremblay, B., Brunette, C., & Newton, R. (2021, May). A Regional Seasonal Forecast Model of Arctic Minimum Sea Ice Extent: Reflected Solar Radiation vs. Late Winter Coastal Divergence. *Journal of Climate*, *-1*(aop), 1–1. Retrieved 2021-06-10, from https://journals.ametsoc.org/view/journals/clim/aop/JCLI-D-20-0846.1/JCLI-D-20-0846.1.xml (Publisher: American Meteorological Society Section: Journal of Climate) doi: 10.1175/JCLI-D-20-0846.1

Krishfield, R., Toole, J., Proshutinsky, A., & Timmermans, M.-L. (2008, November). Automated Ice-Tethered Profilers for Seawater Observations under Pack Ice in All Seasons. *Journal of Atmospheric and Oceanic Technology*, *25*(11), 2091–2105. Retrieved 2021-06-10, from https://journals.ametsoc.org/view/journals/atot/25/11/2008jtecho587_1.xml (Publisher: American Meteorological Society Section: Journal of Atmospheric and Oceanic Technology) doi:

10.1175/2008JTECHO587.1

Kwok, R., & Rothrock, D. A. (2009). Decline in Arctic sea ice thickness from submarine and ICESat records: 1958–2008. *Geophysical Research Letters*, *36*(15). Retrieved 2021-05-21, from https://agupubs.onlinelibrary.wiley.com/doi/abs/10.1029/2009GL039035 (_eprint: https://agupubs.onlinelibrary.wiley.com/doi/pdf/10.1029/2009GL039035) doi: https://doi.org/10.1029/2009GL039035

Ladd, C., Mordy, C. W., Salo, S. A., & Stabeno, P. J. (2016). Winter Water Properties and the Chukchi Polynya. *Journal of Geophysical Research: Oceans*, *121*(8), 5516–5534. Retrieved 2021-03-29, from https://agupubs.onlinelibrary.wiley.com/doi/abs/10.1002/2016JC011918 (_eprint: https://agupubs.onlinelibrary.wiley.com/doi/pdf/10.1002/2016JC011918) doi: https://doi.org/10.1002/2016JC011918

Large, W. G., Danabasoglu, G., McWilliams, J. C., Gent, P. R., & Bryan, F. O. (2001, February). Equatorial Circulation of a Global Ocean Climate Model with Anisotropic Horizontal Viscosity. *Journal of Physical Oceanography*, *31*(2), 518–536. Retrieved 2021-06-10, from https://journals.ametsoc.org/view/journals/phoc/31/2/1520-0485_2001_031_0518_ecoago_2.0.co_2.xml (Publisher: American Meteorological Society Section: Journal of Physical Oceanography) doi: 10.1175/1520-0485(2001)031⟨0518:ECOAGO⟩2.0.CO;2

Large, W. G., McWilliams, J. C., & Doney, S. C. (1994). Oceanic vertical mixing: A review and a model with a nonlocal boundary layer parameterization. *Reviews of Geophysics*, *32*(4), 363–403. Retrieved 2020-11-25, from https://agupubs.onlinelibrary.wiley.com/doi/abs/10.1029/94RG01872 (_eprint: https://agupubs.onlinelibrary.wiley.com/doi/pdf/10.1029/94RG01872) doi: https://doi.org/10.1029/94RG01872

Lemke, P., & Manley, T. O. (1984). The seasonal variation of the mixed layer and the pycnocline under polar sea ice. *Journal of Geophysical Research: Oceans*, *89*(C4), 6494–6504. Retrieved 2021-06-15, from https://agupubs.onlinelibrary.wiley.com/doi/abs/10.1029/JC089iC04p06494 (_eprint: https://agupubs.onlinelibrary.wiley.com/doi/pdf/10.1029/JC089iC04p06494) doi: 10.1029/JC089iC04p06494

Lenetsky, J. E., Tremblay, B., Brunette, C., & Meneghello, G. (2021, June). Subseasonal Predictability of Arctic Ocean Sea Ice Conditions: Bering Strait and Ekman-Driven Ocean Heat Transport. *Journal of Climate*, *34*(11), 4449–4462. Retrieved 2021-05-14, from https://journals.ametsoc.org/view/journals/clim/34/11/JCLI-D-20-0544.1.xml (Publisher: American Meteorological Society Section: Journal of Climate) doi: 10.1175/JCLI-D-20-0544.1

Leonard, B. P. (1979, June). A stable and accurate convective modelling procedure based on quadratic upstream interpolation. *Computer Methods in Applied Mechanics and Engineering*, *19*(1), 59–98. Retrieved 2021-06-10, from https://www.sciencedirect.com/science/article/pii/0045782579900343 doi: 10.1016/0045-7825(79)90034-3

Lipscomb, W. H. (2001). Remapping the thickness distribution in sea ice models. *Journal of Geophysical Research: Oceans*, *106*(C7), 13989–14000. Retrieved 2021-06-10, from https://agupubs.onlinelibrary.wiley.com/doi/abs/10.1029/2000JC000518 (_eprint: https://agupubs.onlinelibrary.wiley.com/doi/pdf/10.1029/2000JC000518) doi: 10.1029/2000JC000518

Manley, T., & Hunkins, K. (1985). Mesoscale eddies of the Arctic Ocean. *J. Geophys. Res.*, *90*(C3), 4911–4930.

Martinson, D. G. (1990). Evolution of the southern ocean winter mixed layer and sea ice: Open ocean deepwater formation and ventilation. *Journal of Geophysical Research: Oceans*, *95*(C7), 11641–11654. Retrieved 2021-05-17, from https://agupubs.onlinelibrary

.wiley.com/doi/abs/10.1029/JC095iC07p11641 (_eprint: https://agupubs.onlinelibrary.wiley.com/doi/pdf/10.1029/JC095iC07p11641) doi: https://doi.org/10.1029/JC095iC07p11641

Maslowski, W., Clement Kinney, J., Higgins, M., & Roberts, A. (2012, May). The Future of Arctic Sea Ice. *Annual Review of Earth and Planetary Sciences*, *40*(1), 625–654. Retrieved 2021-05-17, from https://www.annualreviews.org/doi/10.1146/annurev-earth-042711-105345 (Publisher: Annual Reviews) doi: 10.1146/annurev-earth-042711-105345

Maykut, G. A., & McPhee, M. G. (1995). Solar heating of the Arctic mixed layer. *Journal of Geophysical Research: Oceans*, *100*(C12), 24691–24703. Retrieved 2020-09-24, from https://agupubs.onlinelibrary.wiley.com/doi/abs/10.1029/95JC02554 (_eprint: https://agupubs.onlinelibrary.wiley.com/doi/pdf/10.1029/95JC02554) doi: 10.1029/95JC02554

Maykut, G. A., & Untersteiner, N. (1971). Some results from a time-dependent thermodynamic model of sea ice. *Journal of Geophysical Research (1896-1977)*, *76*(6), 1550–1575. Retrieved 2020-09-24, from https://agupubs.onlinelibrary.wiley.com/doi/abs/10.1029/JC076i006p01550 (_eprint: https://agupubs.onlinelibrary.wiley.com/doi/pdf/10.1029/JC076i006p01550) doi: 10.1029/JC076i006p01550

McLaughlin, F., Carmack, E., Proshutinsky, A., Krishfield, R., Guay, C., Yamamoto-Kawai, M., ... Williams, B. (2011, September). The Rapid Response of the Canada Basin to Climate Forcing: From Bellwether to Alarm Bells. *Oceanography*, *24*(3), 146–159. Retrieved 2020-11-03, from https://tos.org/oceanography/article/the-rapid-response-of-the-canada-basin-to-climate-forcing-from-bellwether-t doi: 10.5670/oceanog.2011.66

Meneghello, G., Doddridge, E., Marshall, J., Scott, J., & Campin, J.-M. (2020, January). Exploring the Role of the "Ice–Ocean Governor" and Mesoscale Eddies in the Equilibration of the Beaufort Gyre: Lessons from Observations. *Journal of Physical Oceanography*, *50*(1), 269–277. Retrieved 2021-02-01, from https://journals.ametsoc.org/view/journals/phoc/50/1/jpo-d-18-0223.1.xml doi: 10.1175/JPO-D-18-0223.1

Meneghello, G., Marshall, J., Campin, J.-M., Doddridge, E., & Timmermans, M.-L. (2018). The Ice-Ocean Governor: Ice-Ocean Stress Feedback Limits Beaufort Gyre Spin-Up. *Geophysical Research Letters*, *45*(20), 11,293–11,299. Retrieved 2021-02-01, from https://agupubs.onlinelibrary.wiley.com/doi/abs/10.1029/2018GL080171 (_eprint: https://agupubs.onlinelibrary.wiley.com/doi/pdf/10.1029/2018GL080171) doi: https://doi.org/10.1029/2018GL080171

Meneghello, G., Marshall, J., Timmermans, M.-L., & Scott, J. (2018, April). Observations of Seasonal Upwelling and Downwelling in the Beaufort Sea Mediated by Sea Ice. *American Meteorological Society*. Retrieved 2020-09-24, from https://dspace.mit.edu/handle/1721.1/118476 (Accepted: 2018-10-15T14:57:15Z Publisher: American Meteorological Society)

Mlawer, E. J., Taubman, S. J., Brown, P. D., Iacono, M. J., & Clough, S. A. (1997). Radiative transfer for inhomogeneous atmospheres: RRTM, a validated correlated-k model for the longwave. *Journal of Geophysical Research: Atmospheres*, *102*(D14), 16663–16682. Retrieved 2021-06-10, from https://agupubs.onlinelibrary.wiley.com/doi/abs/10.1029/97JD00237 (_eprint: https://agupubs.onlinelibrary.wiley.com/doi/pdf/10.1029/97JD00237) doi: 10.1029/97JD00237

Morison, J., & Smith, J. D. (1981). Seasonal variations in the upper Arctic Ocean as observed at T-3. *Geophysical Research Letters*, *8*(7), 753–756. Retrieved 2021-06-15, from https://agupubs.onlinelibrary.wiley.com/doi/abs/10.1029/GL008i007p00753 (_eprint:

https://agupubs.onlinelibrary.wiley.com/doi/pdf/10.1029/GL008i007p00753) doi: 10.1029/GL008i007p00753

Moritz, Richard. (2020). *Salinity, Temperature, Depth profiler data at AIDJEX stations April 1975 through April 1976, Version 1.* CanWIN: Canadian Watershed Information Network. Retrieved from https://doi.org/10.34992/4xak-8r05

Nguyen, A. T., Menemenlis, D., & Kwok, R. (2009). Improved modeling of the Arctic halocline with a subgrid-scale brine rejection parameterization. *Journal of Geophysical Research: Oceans*, *114*(C11). Retrieved 2020-09-25, from https://agupubs.onlinelibrary.wiley.com/doi/abs/10.1029/2008JC005121 (_eprint: https://agupubs.onlinelibrary.wiley.com/doi/pdf/10.1029/2008JC005121) doi: 10.1029/2008JC005121

Nikolopoulos, A., Pickart, R. S., Fratantoni, P. S., Shimada, K., Torres, D. J., & Jones, E. P. (2009, August). The western Arctic boundary current at 152°W: Structure, variability, and transport. *Deep Sea Research Part II: Topical Studies in Oceanography*, *56*(17), 1164–1181. Retrieved 2021-03-29, from https://www.sciencedirect.com/science/article/pii/S0967064508003445 doi: 10.1016/j.dsr2.2008.10.014

Niu, G.-Y., Yang, Z.-L., Dickinson, R. E., & Gulden, L. E. (2005). A simple TOPMODEL-based runoff parameterization (SIMTOP) for use in global climate models. *Journal of Geophysical Research*, *110*(D21), D21106. Retrieved 2021-05-04, from http://doi.wiley.com/10.1029/2005JD006111 doi: 10.1029/2005JD006111

Ohlmann, J. C. (2003, May). Ocean Radiant Heating in Climate Models. *Journal of Climate*, *16*(9), 1337–1351. Retrieved 2020-10-28, from https://journals.ametsoc.org/jcli/article/16/9/1337/30002/Ocean-Radiant-Heating-in-Climate-Models (Publisher: American Meteorological Society) doi: 10.1175/1520-0442-16.9.1337

Peralta-Ferriz, C., & Woodgate, R. A. (2015, May). Seasonal and interannual variability of pan-Arctic surface mixed layer properties from 1979 to 2012 from hydrographic data, and the dominance of stratification for multiyear mixed layer depth shoaling. *Progress in Oceanography*, *134*, 19–53. Retrieved 2020-09-24, from http://www.sciencedirect.com/science/article/pii/S0079661114002158 doi: 10.1016/j.pocean.2014.12.005

Perovich, D. K., Jones, K. F., Light, B., Eicken, H., Markus, T., Stroeve, J., & Lindsay, R. (2011). Solar partitioning in a changing Arctic sea-ice cover. *Annals of Glaciology*, *52*(57), 192–196. Retrieved 2020-09-24, from https://www.cambridge.org/core/journals/annals-of-glaciology/article/solar-partitioning-in-a-changing-arctic-seaice-cover/363DD9F8A62A5D542B58B4C6D543E45D (Publisher: Cambridge University Press) doi: 10.3189/172756411795931543

Perovich, D. K., Light, B., Eicken, H., Jones, K. F., Runciman, K., & Nghiem, S. V. (2007). Increasing solar heating of the Arctic Ocean and adjacent seas, 1979–2005: Attribution and role in the ice-albedo feedback. *Geophysical Research Letters*, *34*(19). Retrieved 2020-09-24, from https://agupubs.onlinelibrary.wiley.com/doi/abs/10.1029/2007GL031480 (_eprint: https://agupubs.onlinelibrary.wiley.com/doi/pdf/10.1029/2007GL031480) doi: 10.1029/2007GL031480

Perovich, D. K., & Richter-Menge, J. A. (2015, July). Regional variability in sea ice melt in a changing Arctic. *Philosophical Transactions of the Royal Society A: Mathematical, Physical and Engineering Sciences*, *373*(2045), 20140165. Retrieved 2021-02-09, from https://royalsocietypublishing.org/doi/full/10.1098/rsta.2014.0165 (Publisher: Royal Society) doi: 10.1098/rsta.2014.0165

Perovich, D. K., Richter-Menge, J. A., Jones, K. F., Light, B., Elder, B. C., Polashenski, C., ... Lindsay, R. (2011). Arctic sea-ice melt in 2008 and the role of solar heating. *Annals of Glaciology*, *52*(57), 355–359. Retrieved 2020-09-24, from https://www.cambridge.org/core/journals/annals-of-glaciology/article/arctic-seaice-melt-in-2008-and-the-role-of-solar-heating/D897CF2FB0ABF20528C40976DA689B99 (Publisher: Cambridge University Press) doi: 10.3189/172756411795931714

Perovich, D. K., Richter-Menge, J. A., Jones, K. F., & Light, B. (2008). Sunlight, water, and ice: Extreme Arctic sea ice melt during the summer of 2007. *Geophysical Research Letters*, *35*(11). Retrieved 2020-09-24, from https://agupubs.onlinelibrary.wiley.com/doi/abs/10.1029/2008GL034007 (_eprint: https://agupubs.onlinelibrary.wiley.com/doi/pdf/10.1029/2008GL034007) doi: 10.1029/2008GL034007

Perovich, D., J. Richter-Menge, & C. Polashenski. (2021). *Observing and understanding climate change: Monitoring the mass balance, motion, and thickness of Arctic sea ice.* Retrieved 2021-02-19, from http://imb-crrel-dartmouth.org/archived-data/

Peterson, A. K., Fer, I., McPhee, M. G., & Randelhoff, A. (2017). Turbulent heat and momentum fluxes in the upper ocean under Arctic sea ice. *Journal of Geophysical Research: Oceans*, *122*(2), 1439–1456. Retrieved 2021-05-07, from https://agupubs.onlinelibrary.wiley.com/doi/abs/10.1002/2016JC012283 (_eprint: https://agupubs.onlinelibrary.wiley.com/doi/pdf/10.1002/2016JC012283) doi: https://doi.org/10.1002/2016JC012283

Petty, A. A., Hutchings, J. K., Richter-Menge, J. A., & Tschudi, M. A. (2016). Sea ice circulation around the Beaufort Gyre: The changing role of wind forcing and the sea ice state. *Journal of Geophysical Research: Oceans*, *121*(5), 3278–3296. Retrieved 2021-05-20, from https://agupubs.onlinelibrary.wiley.com/doi/abs/10.1002/2015JC010903 (_eprint: https://agupubs.onlinelibrary.wiley.com/doi/pdf/10.1002/2015JC010903) doi: https://doi.org/10.1002/2015JC010903

Pickart, R. S. (2004, April). Shelfbreak circulation in the Alaskan Beaufort Sea: Mean structure and variability. *Journal of Geophysical Research: Oceans*, *109*(C4). Retrieved 2021-03-29, from https://agupubs.onlinelibrary.wiley.com/doi/full/10.1029/2003JC001912 (Publisher: John Wiley & Sons, Ltd) doi: 10.1029/2003JC001912

Pickart, R. S., Weingartner, T. J., Pratt, L. J., Zimmermann, S., & Torres, D. J. (2005, December). Flow of winter-transformed Pacific water into the Western Arctic. *Deep Sea Research Part II: Topical Studies in Oceanography*, *52*(24), 3175–3198. Retrieved 2021-03-29, from https://www.sciencedirect.com/science/article/pii/S096706450500216X doi: 10.1016/j.dsr2.2005.10.009

Proshutinsky, A., Krishfield, R., Timmermans, M.-L., Toole, J., Carmack, E., McLaughlin, F., ... Shimada, K. (2009). Beaufort Gyre freshwater reservoir: State and variability from observations. *Journal of Geophysical Research: Oceans*, *114*(C1). Retrieved 2020-09-24, from https://agupubs.onlinelibrary.wiley.com/doi/abs/10.1029/2008JC005104 (_eprint: https://agupubs.onlinelibrary.wiley.com/doi/pdf/10.1029/2008JC005104) doi: 10.1029/2008JC005104

Rainville, L., Lee, C. M., & Woodgate, R. A. (2011). Impact of Wind-Driven Mixing in the Arctic Ocean. *Oceanography*, *24*(3), 136–145. Retrieved 2021-05-17, from https://www.jstor.org/stable/24861308 (Publisher: Oceanography Society)

Rosenblum, E., & Eisenman, I. (2017, August). Sea Ice Trends in Climate Models Only Accurate in Runs with Biased Global Warming. *Journal*

of Climate, *30*(16), 6265–6278. Retrieved 2021-06-29, from https://journals.ametsoc.org/view/journals/clim/30/16/jcli-d-16-0455.1.xml (Publisher: American Meteorological Society Section: Journal of Climate) doi: 10.1175/JCLI-D-16-0455.1

Rosenblum, E., Fajber, R., Stroeve, J., Gille, S., Tremblay, B., & Carmack, E. (2021, June). *Surface salinity under transitioning ice cover in the Canada Basin: Climate model biases linked to vertical 2 distribution of freshwater* (preprint). Oceanography. Retrieved 2021-06-15, from http://www.essoar.org/doi/10.1002/essoar.10507260.1 doi: 10.1002/essoar.10507260.1

Rosenblum, E., Stroeve, J., Gille, S. T., Tremblay, L. B., Lique, C., Fajber, R., ... Lukovich, J. (2021, February). *Freshwater input and vertical mixing in the Canada Basin's seasonal halocline: 1975 vs 2006-2012* [preprint]. Retrieved 2021-06-15, from http://www.essoar.org/doi/10.1002/essoar.10507192.1 (Archive Location: world Publisher: Earth and Space Science Open Archive Section: Oceanography) doi: 10.1002/essoar.10507192.1

Rudels, B., Anderson, L. G., & Jones, E. P. (1996). Formation and evolution of the surface mixed layer and halocline of the Arctic Ocean. *Journal of Geophysical Research: Oceans*, *101*(C4), 8807–8821. Retrieved 2020-09-25, from https://agupubs.onlinelibrary.wiley.com/doi/abs/10.1029/96JC00143 (_eprint: https://agupubs.onlinelibrary.wiley.com/doi/pdf/10.1029/96JC00143) doi: 10.1029/96JC00143

Shaw, W. J., & Stanton, T. P. (2014). Vertical diffusivity of the Western Arctic Ocean halocline. *Journal of Geophysical Research: Oceans*, *119*(8), 5017–5038. Retrieved 2020-09-24, from https://agupubs.onlinelibrary.wiley.com/doi/abs/10.1002/2013JC009598 (_eprint: https://agupubs.onlinelibrary.wiley.com/doi/pdf/10.1002/2013JC009598) doi: 10.1002/2013JC009598

Steele, M., & Boyd, T. (1998). Retreat of the cold halocline layer in the Arctic Ocean. *Journal of Geophysical Research: Oceans*, *103*(C5), 10419–10435. Retrieved 2021-03-22, from https://agupubs.onlinelibrary.wiley.com/doi/abs/10.1029/98JC00580 (_eprint: https://agupubs.onlinelibrary.wiley.com/doi/pdf/10.1029/98JC00580) doi: https://doi.org/10.1029/98JC00580

Steele, M., Ermold, W., & Zhang, J. (2011). Modeling the formation and fate of the near-surface temperature maximum in the Canadian Basin of the Arctic Ocean. *Journal of Geophysical Research: Oceans*, *116*(C11). Retrieved 2021-03-25, from https://agupubs.onlinelibrary.wiley.com/doi/abs/10.1029/2010JC006803 (_eprint: https://agupubs.onlinelibrary.wiley.com/doi/pdf/10.1029/2010JC006803) doi: https://doi.org/10.1029/2010JC006803

Steele, M., Zhang, J., & Ermold, W. (2010). Mechanisms of summertime upper Arctic Ocean warming and the effect on sea ice melt. *Journal of Geophysical Research: Oceans*, *115*(C11). Retrieved 2021-05-14, from https://agupubs.onlinelibrary.wiley.com/doi/abs/10.1029/2009JC005849 (_eprint: https://agupubs.onlinelibrary.wiley.com/doi/pdf/10.1029/2009JC005849) doi: https://doi.org/10.1029/2009JC005849

Timmermans, M.-L. (2015). The impact of stored solar heat on Arctic sea ice growth. *Geophysical Research Letters*, *42*(15), 6399–6406. Retrieved 2021-06-15, from https://agupubs.onlinelibrary.wiley.com/doi/abs/10.1002/2015GL064541 (_eprint: https://agupubs.onlinelibrary.wiley.com/doi/pdf/10.1002/2015GL064541) doi: 10.1002/2015GL064541

Timmermans, M.-L., Toole, J., Krishfield, R., & Winsor, P. (2008). Ice-Tethered Profiler observations of the double-diffusive staircase in the Canada Basin thermocline. *Journal of Geophysical Research:*

Oceans, *113*(C1). Retrieved 2021-03-25, from https://agupubs.onlinelibrary.wiley.com/doi/abs/10.1029/2008JC004829 (_eprint: https://agupubs.onlinelibrary.wiley.com/doi/pdf/10.1029/2008JC004829) doi: https://doi.org/10.1029/2008JC004829

Toole, J. M., Timmermans, M.-L., Perovich, D. K., Krishfield, R. A., Proshutinsky, A., & Richter-Menge, J. A. (2010). Influences of the ocean surface mixed layer and thermohaline stratification on Arctic Sea ice in the central Canada Basin. *Journal of Geophysical Research: Oceans*, *115*(C10). Retrieved 2021-04-01, from https://agupubs.onlinelibrary.wiley.com/doi/abs/10.1029/2009JC005660 (_eprint: https://agupubs.onlinelibrary.wiley.com/doi/pdf/10.1029/2009JC005660) doi: https://doi.org/10.1029/2009JC005660

Untersteiner, N. (1961, January). On the mass and heat budget of arctic sea ice. *Archiv für Meteorologie, Geophysik und Bioklimatologie Serie A*, *12*(2), 151–182. Retrieved 2021-02-08, from http://link.springer.com/10.1007/BF02247491 doi: 10.1007/BF02247491

Weingartner, T., Aagaard, K., Woodgate, R., Danielson, S., Sasaki, Y., & Cavalieri, D. (2005, December). Circulation on the north central Chukchi Sea shelf. *Deep Sea Research Part II: Topical Studies in Oceanography*, *52*(24), 3150–3174. Retrieved 2021-03-29, from https://www.sciencedirect.com/science/article/pii/S0967064505002158 doi: 10.1016/j.dsr2.2005.10.015

Woodgate, R. A., Weingartner, T., & Lindsay, R. (2010). The 2007 Bering Strait oceanic heat flux and anomalous Arctic sea-ice retreat. *Geophysical Research Letters*, *37*(1). Retrieved 2021-05-14, from https://agupubs.onlinelibrary.wiley.com/doi/abs/10.1029/2009GL041621 (_eprint: https://agupubs.onlinelibrary.wiley.com/doi/pdf/10.1029/2009GL041621) doi: https://doi.org/10.1029/2009GL041621

Yamamoto-Kawai, M., McLaughlin, F. A., Carmack, E. C., Nishino, S., & Shimada, K. (2008). Freshwater budget of the Canada Basin, Arctic Ocean, from salinity, delta 18O, and nutrients. *Journal of Geophysical Research: Oceans*, *113*(C1). Retrieved 2021-03-22, from https://agupubs.onlinelibrary.wiley.com/doi/abs/10.1029/2006JC003858 (_eprint: https://agupubs.onlinelibrary.wiley.com/doi/pdf/10.1029/2006JC003858) doi: https://doi.org/10.1029/2006JC003858

Zhang, J., & Steele, M. (2007). Effect of vertical mixing on the Atlantic Water layer circulation in the Arctic Ocean. *Journal of Geophysical Research: Oceans*, *112*(C4). Retrieved 2021-02-04, from https://agupubs.onlinelibrary.wiley.com/doi/abs/10.1029/2006JC003732 (_eprint: https://agupubs.onlinelibrary.wiley.com/doi/pdf/10.1029/2006JC003732) doi: https://doi.org/10.1029/2006JC003732

Table 1. Names of the CESM-LE variables.

Variables	CESM-LE (POP)	CESM-LE (CICE)
Θ	TEMP	-
S	SALT	-
F_{hor}	ADVT + HDIFT	-
F_{io}	MELTH_F	fhocn_ai
F_{frazil}	QFLUX	-
F_{lw}	LWDN_F+LWUP_F	-
F_{sens}	SENH_F	-
F_{evap}	EVAP_F$\times$ latent_heat_vapor	-
$F_{sw}(z=0)$	SHF_QSW	-
$F_{sw,io}(z=0)$	-	fswthru_ai
$F_{sw}(z)$	QSW_3D	-
$\left.\frac{\partial h}{\partial t}\right\|_{\mathrm{t}}$	-	-meltt
$\left.\frac{\partial h}{\partial t}\right\|_{\mathrm{b,l}}$	-	-meltb-meltl+congel
$\left.\frac{\partial h}{\partial t}\right\|_{\mathrm{f}}$	-	frazil
F_{ct}	-	fcondtop_ai
F_{cb}	-	-((congel-meltb-meltl)*rho_ice*latent_heat_fusion)
$F_{sw,ai}$	-	fswabs_ai
$F_{lw,ai}$	-	flwup_ai + (aice $\times$ flwdn)
F_{sens_ai}	-	fsens_ai
F_{lat_ai}	-	flat_ai
$w\Theta$	WTT Δz	-
$-\frac{\partial(wE)}{\partial z}$	$-\Delta$ WTT $c_p\rho$	-
$\frac{\partial}{\partial z}\kappa\frac{\partial\Theta}{\partial z}$	$\frac{\Delta\text{DIA_IMPVF_TEMP}}{\Delta z}$	-
$-\frac{\partial}{\partial z}\kappa\gamma_\Theta$	KPP_SRC_TEMP	-
$D_{v,GM}(\Theta)$	ΔHDIFB_TEMP	-